Molecular Cell
Resource

The Complexity of Human Ribosome Biogenesis Revealed by Systematic Nucleolar Screening of Pre-rRNA Processing Factors

Lionel Tafforeau,[1,2] Christiane Zorbas,[1,2] Jean-Louis Langhendries,[1] Sahra-Taylor Mullineux,[1] Vassiliki Stamatopoulou,[1] Romain Mullier,[1] Ludivine Wacheul,[1] and Denis L.J. Lafontaine[1,*]
[1]Fonds de la Recherche Scientifique (FRS-FNRS), Université Libre de Bruxelles (ULB), 1050 Bruxelles, Belgium
[2]These authors contributed equally to this work
*Correspondence: denis.lafontaine@ulb.ac.be
http://dx.doi.org/10.1016/j.molcel.2013.08.011

SUMMARY

Mature ribosomal RNAs (rRNAs) are produced from polycistronic precursors following complex processing. Precursor (pre)-rRNA processing has been extensively characterized in yeast and was assumed to be conserved in humans. We functionally characterized 625 nucleolar proteins in HeLa cells and identified 286 required for processing, including 74 without a yeast homolog. For selected candidates, we demonstrated that pre-rRNA processing defects are conserved in different cell types (including primary cells), defects are not due to activation of a p53-dependent nucleolar tumor surveillance pathway, and they precede cell-cycle arrest and apoptosis. We also investigated the exosome's role in processing internal transcribed spacers (ITSs) and report that 3′ end maturation of 18S rRNA involves EXOSC10/Rrp6, a yeast ITS2 processing factor. We conclude that human cells adopt unique strategies and recruit distinct *trans*-acting factors to carry out essential processing steps, posing fundamental implications for understanding ribosomopathies at the molecular level and developing effective therapeutic agents.

INTRODUCTION

The nucleolus is a prominent nuclear organelle, central to gene expression, in which ribosome synthesis is initiated (Boisvert et al., 2007). Ribosome synthesis is fundamental to all life forms, and the sequences of mature ribosomal RNAs (rRNAs) and the overall structure of the ribosome are evolutionarily conserved. The nucleolus is a potent biomarker of cellular health; alterations in morphology and protein content are indicators of changes in cell growth and proliferation, cell-cycle regulation and senescence, as well as stress responses and cancer (Boulon et al., 2010; Ruggero and Pandolfi, 2003). A class of human diseases was recently designated as ribosomopathies; these are inherited or somatically acquired human syndromes characterized by impaired hematopoiesis and increased cancer susceptibility. They are associated with mutations in genes encoding ribosomal components, typically leading to haploinsufficiency of ribosomal proteins, or mutations in ribosome assembly factors. Ribosomopathies include Diamond-Blackfan anemia (DBA), Schwachman-Diamond and Treacher Collins syndromes, X-linked dyskeratosis congenita (X-DC), T cell acute lymphoblastic leukemia, and isolated congenital asplenia, among others (Farrar et al., 2011; Johnson and Ellis, 2011; Narla and Ebert, 2011; De Keersmaecker et al., 2013; Bolze et al., 2013).

The nucleolus is not membrane bound and can adopt an extremely dynamic structure; nucleolar morphology may vary greatly depending on the growth conditions and physiological status of the cell (Dimario, 2004). Several years ago, plant and mammalian nucleoli were purified, and their protein content was established by mass spectrometry (Andersen et al., 2002; Pendle et al., 2005; Scherl et al., 2002). The initial analysis in HeLa cells revealed that the nucleolus contains ~700 abundant proteins (compared to ~150 nucleolar proteins identified in budding yeast, based on high-throughput localization of GFP fusions; Huh et al., 2003). With the increased sensitivity of mass spectrometry techniques, this estimate was raised to ~4,500 putative nucleolar proteins (Ahmad et al., 2009). The mammalian nucleolar proteome was first established under a near-physiological state, and it was later analyzed under stress conditions such as drug-induced transcriptional shutdown, adenovirus infection, and UV and ionizing irradiation (Andersen et al., 2005; Lam et al., 2010; Moore et al., 2011). These studies demonstrated the highly fluctuating nature of the nucleolar proteome, confirming the results from earlier light microscopy studies (Olson and Dundr, 2005; Phair and Misteli, 2000).

Four rRNAs lay at the core of the eukaryotic ribosome, three of which are produced by the extensive processing of a polycistronic rRNA transcript (47S in humans), synthesized by RNA polymerase (Pol) I (reviewed in Mullineux and Lafontaine, 2012). The 5S rRNA, part of the large ribosomal subunit, is transcribed separately by RNA Pol III. In human cells, processing of the 47S primary transcript follows one of two pathways (Figure S1 available online) and encompasses numerous cleavage reactions to remove external and internal spacers. Pre-rRNA processing is only one of the many facets of ribosome synthesis; however, it is highly integrated with other steps, such as covalent modification of ribosomal components and binding of ribosome

assembly factors and ribosomal proteins (Lafontaine, 2010). Pre-rRNA maturation involves the sequential generation of intermediate RNA species, many of which are readily detectable by high-resolution northern blots. Ribosome biogenesis entails maturation steps in the nucleolus, nucleoplasm, and cytoplasm, where final processing of both the small and large ribosomal subunit rRNAs occurs. Analysis of pre-rRNA processing, therefore, provides a straightforward and well-resolved readout, both temporally and spatially, of ribosome synthesis.

In an effort to better understand ribosome synthesis in humans, we characterized the role in pre-rRNA processing of a selection of 625 putative nucleolar proteins in HeLa cells, identifying 286 pre-rRNA processing factors, including 74 without a yeast homolog. For a selection of candidates, we show that the pre-rRNA processing defects observed are remarkably similar in different cell types, including primary cells, that they are not p53-dependent, and that they largely precede other cellular phenotypes, such as cell-cycle arrest and programmed cell death. For many years, ribosome research in mammals has lagged behind that of budding yeast. This is largely because yeast genetics (e.g., synthetic lethality and suppressor screens) and pre-ribosome purification by tandem affinity chromatography proved extremely powerful for the identification of the >200 ribosome synthesis *trans*-acting factors identified to date in this experimental model. This is also a reflection of the largely acknowledged assumption, mostly based on sequence conservation of the putative human homologs of known yeast assembly factors, that ribosome synthesis is largely conserved throughout eukaryotes. We provide initial, but compelling, evidence that calls this concept into question: ~27% of the human factors have either distinct or additional functions in pre-rRNA processing as compared to their yeast orthologs. We show that EXOSC10 (yeast Rrp6), which functions in 3′ end maturation of the yeast 5.8S rRNA (internal transcribed spacer 2 [ITS2] processing), is also involved in processing the 3′ end of 18S rRNA (ITS1 processing) in human cells. This conclusion has important consequences for both understanding ribosomopathies at the molecular level and identifying potential therapeutic targets.

RESULTS

Rationale of the Screening Procedure

Based on the nucleolar proteomes recently described in humans, bovine, and plants, we assembled a list of genes with putative functions in pre-rRNA processing and experimentally tested 625 candidates in HeLa cells (Table S1). The messenger RNA (mRNA) for each was depleted over 3 days with one of three short interfering RNA (siRNA); the experimental approach is outlined in Figure 1A. Total RNA was extracted, separated on denaturing agarose gels, and analyzed by northern blotting. The probes, complementary to the 5′ external transcribed spacer (ETS), ITS1, and ITS2, hybridize to all known normal, as well as some aberrant, pre-rRNA intermediates (Figures 1B, 1C, and S1). For each set of depletions, a nontargeting siRNA (scrambled, SCR) and calibration controls were included (Figure 1C). The calibration set comprised four model genes: *NOL9*, *RPS3*, *RPS11*, and *UTP18*. These are processing factors for which their depletion results in the accumulation or reduction of certain normal or aberrant pre-rRNA intermediates, and they were selected for their involvement in specific reactions in the pre-rRNA processing pathway (Heindl and Martinez, 2010; Hölzel et al., 2010; O'Donohue et al., 2010). For example, cells depleted for UTP18 accumulate the aberrant 34S RNA, resulting from inhibition of early cleavage reactions (at sites 01, A0, and 1). Cells deprived of RPS11 strongly accumulate the 30S pre-rRNA due to a lack of processing at A0 and 1. NOL9 is primarily involved in ITS2 processing, since the 32S pre-rRNA accumulates in its absence. The 43S and the 26S pre-rRNAs are detected in cells depleted for RPS3 in higher amounts than in untreated cells, revealing an uncoupling of cleavage at sites A0 and 1 (see Mullineux and Lafontaine, 2012 for further discussion). In cells deprived of RPS3, our high-resolution analysis also showed an accumulation of 21S-C, a trimmed version of 21S and late precursor in the 18S rRNA maturation pathway (Figure S1).

The calibration set was included in each batch of siRNA transfection experiments and northern hybridizations in order to technically validate the siRNA depletions and unambiguously identify pre-rRNA intermediates. Each prominent intermediate detected was quantitated (heatmap in Figure 1C), and the data set, representing 1,875 siRNA depletions (excluding controls), was assembled into a matrix and integrated with a clustering software (see www.ribogenesis.com and Experimental Procedures). Proteins whose depletion produced similar patterns of accumulation or reduction of pre-rRNA precursors ("pre-rRNA profile") were automatically clustered. We designated specific functional classes on the basis of the observed patterns (Figure 2A). The reiterative controls of the calibration set, repeated >50 times, reproducibly clustered in the same groups (data not shown).

Functional Clustering and Emerging Classes of Ribosome Synthesis *trans*-Acting Factors

In order to assess the efficiency of siRNA-mediated depletions, we determined the relative levels of residual mRNAs for selected siRNAs using a shotgun quantitative PCR (qPCR) approach (Figure S2). We tested 154 siRNAs, ~8% of all inactivations, and found that the level of residual targeted mRNA was <20% for 84 siRNAs tested, 20%–40% for 49 siRNAs, and 40%–60% for 16 siRNAs. Out of the 26 genes in the qPCR assay for which we tested three siRNAs, we found that for two genes only one of the siRNAs failed to efficiently deplete the target mRNA (*NIPBL* and *NOP58*, Figure S2A).

We defined 12 functional classes of assembly factors based on the clustering of the pre-rRNA profiles of depleted proteins (Figure 2A and Tables 1 and S2). Of the 625 proteins analyzed, 70 showed an identical or very similar pre-rRNA profile upon mRNA depletion with all three siRNAs (Table 1). An additional 216 proteins showed an identical or similar profile upon depletion with two of the three siRNAs. Table 1 lists the 286 proteins identified as being strongly required for pre-rRNA processing. These are characterized by a >1.5-fold increase or decrease of at least one of the intermediates. For proteins already described in the literature, we have largely confirmed and extended previously reported phenotypes (Table S10).

Of the 286 proteins, 153 have a yeast homolog known to be a ribosome biogenesis factor, 59 have a yeast homolog not

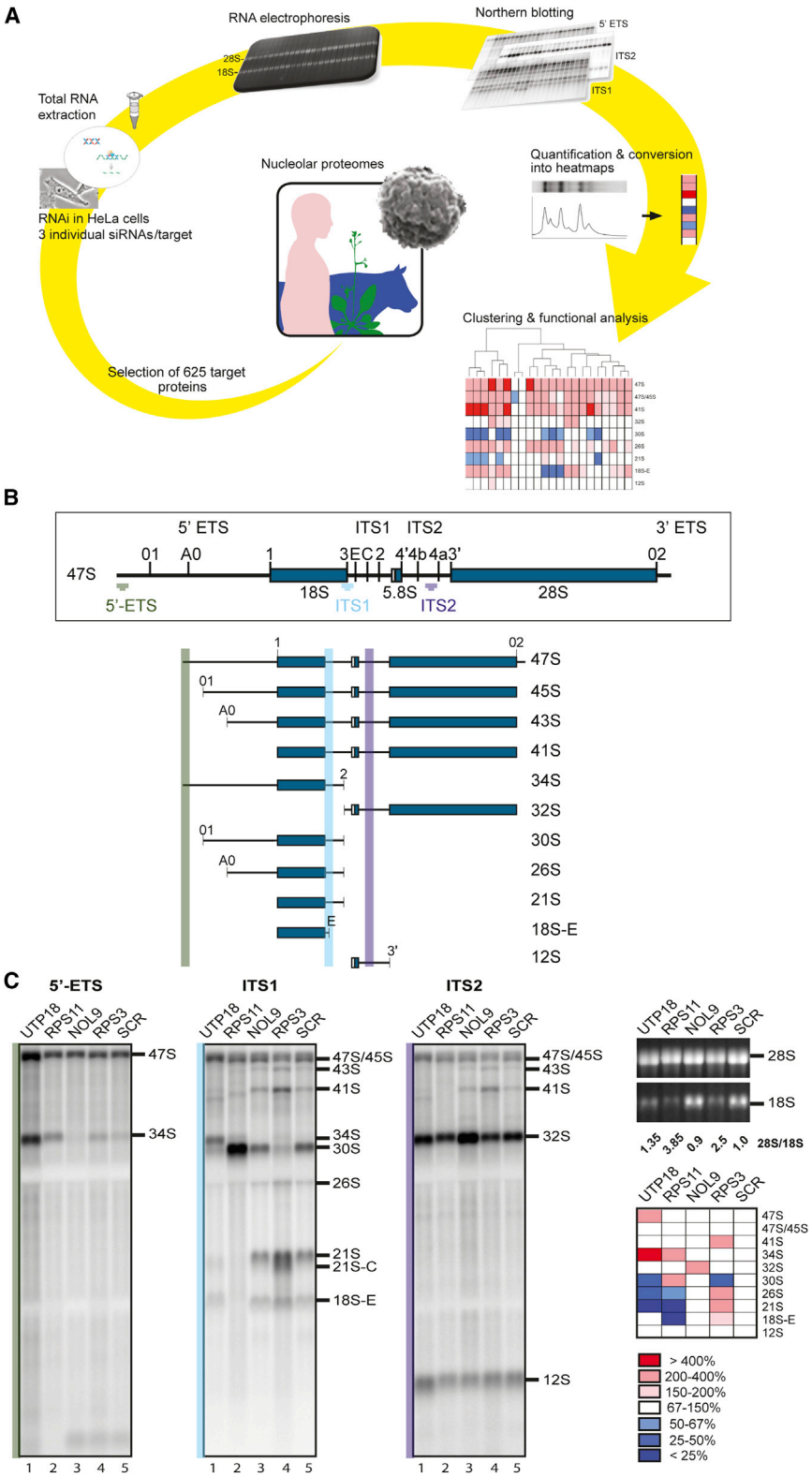

Figure 1. Probing the Human Nucleolar Proteome to Identify Pre-rRNA Processing Factors

(A) Experimental scheme: a list of 625 candidate genes was compiled from the human, bovine, and plant nucleolar proteomes. Each target was depleted in HeLa cells with three unique siRNAs in three independent experiments. Total RNA was extracted and separated by denaturing agarose gel electrophoresis. Gels were transferred to nylon membranes and hybridized with probes (5′ ETS, ITS1, and ITS2; see B), detecting all major pre-rRNA intermediates. Bands were quantitated with a phosphorimager. The data set was assembled into a 1,875 × 10 matrix and analyzed with the clustering software R, generating a rooted tree (see www.ribogenesis.com).

(B) Probing scheme of the northern blots: human rDNA unit and location of probes. The 18S, 5.8S, and 28S rRNA are transcribed by RNA Pol I in a single long transcript, the 47S pre-rRNA. The mature rRNA sequences are flanked with the 5′ ETS and 3′ ETS external transcribed spacers and ITS1 and ITS2 internal spacers (Figure S1). The probes used in the screening (5′ ETS, ITS1, and ITS2; see Table S8), as well as the major pre-cursors detected, are depicted.

(C) A set of calibration controls (NOL9, RPS3, RPS11, UTP18, and nontargeting, SCR) was included to visualize a wide range of pre-rRNA processing defects. Bands on the northern blots were quantitated, and the data set was converted into heatmaps. The color code expresses the percentage of each RNA with respect to the SCR control. The ratio of the mature rRNAs, 28S/18S, was extracted from electropherograms obtained with a Bioanalyzer (Agilent). See also Figure S1 and Tables S1, S7, and S8.

directly linked to ribosome synthesis, and 74 have no obvious yeast homolog (Figure 2B and Tables S3 and S4). Strikingly, many human genes (109/286 genes, 38%) identified in our screen as ribosome assembly factors are also known disease biomarkers, notably in cancer (Figure 2C and Table S5). Several noteworthy examples include *WDR36*, mutated in open-angle glaucoma (Fan et al., 2009); *SIRT7*, over-expressed in breast cancer (Ashraf et al., 2006); *NOL7*, downregulated in cervical cancer (Hasina et al., 2006); *RPF1*, mutated in nephroblastoma (Perotti et al., 2004); *CDKN2A* ($p14^{ARF}$), linked to the p53 pathway (Ozenne et al., 2010); and *GLTSCR2*/*PICT1*, a proto-oncogene (Sasaki et al., 2011). The distributions of ribosome synthesis factors involved in early, intermediate, or late pre-rRNA processing steps, and whether or not they exert a similar function as their yeast counterpart, are shown in Figures 2D and 2E, respectively (Table S6). Given the abundance of the nucleolar proteome, it is not surprising that close to 75% of the factors identified are involved in early pre-rRNA processing

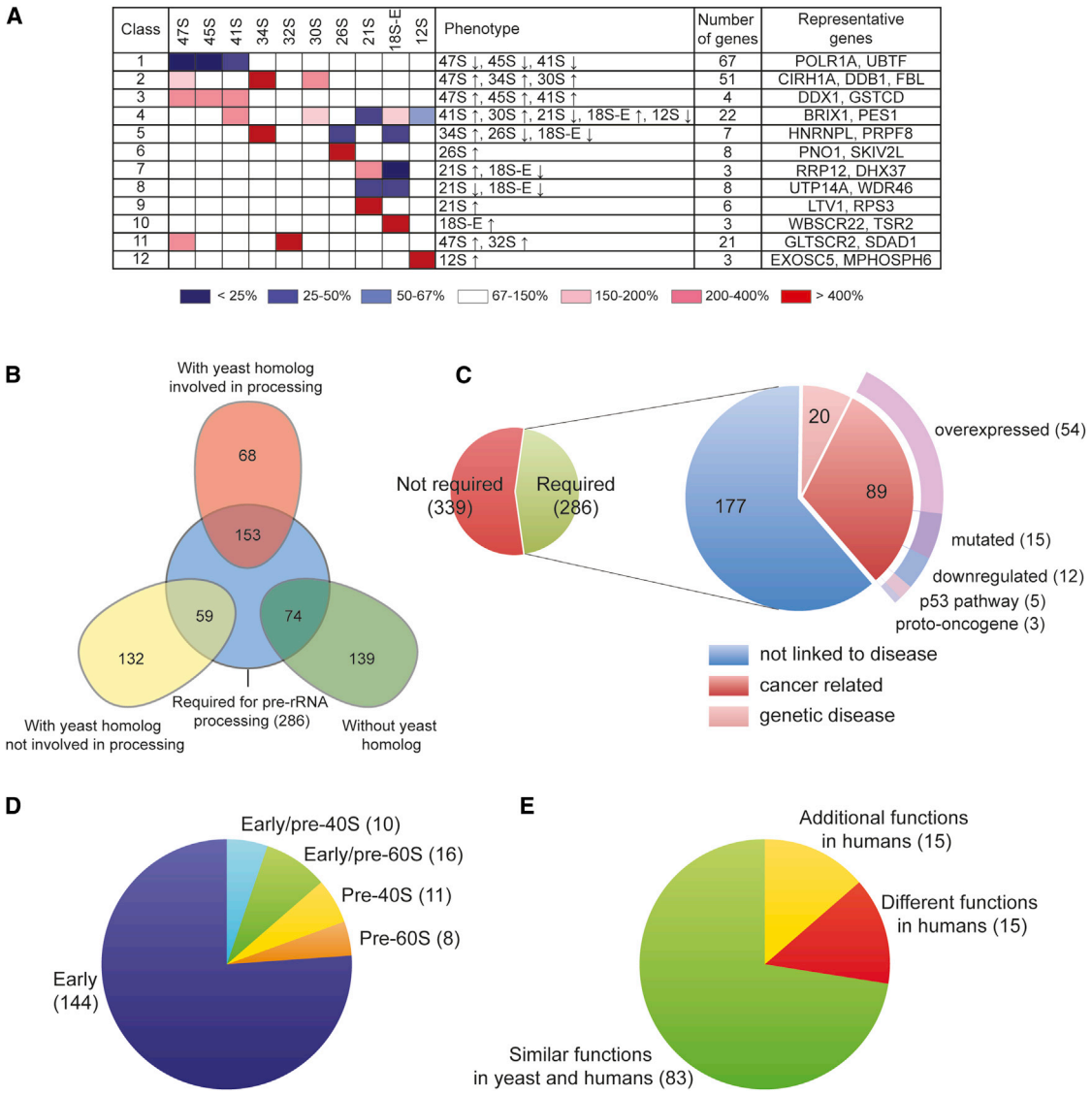

Figure 2. Functional Classes of Human Pre-rRNA Processing Factors

(A) Gene products whose depletion led to a similar pattern of accumulation and/or reduction of pre-rRNAs were grouped into 12 classes (see www.ribogenesis.com for details). The heatmap shows prototypic alterations of the patterns in each class. In this table and on the website, the 45S formally refers to 47S/45S. Key: red, increased-abundance RNAs; blue, decreased-abundance RNAs. The color code expresses the percentage of each RNA with respect to the SCR. The number of genes in each class and examples are indicated (not included: 83 genes defining a miscellaneous family. See Table 1 for details).

(B and C) Venn diagrams showing the distribution of the 286 genes identified as human pre-rRNA processing factors (depletion leads to a >1.5-fold change of at least one pre-rRNA species) into three classes based on the presence or absence of ribosomal processing activity in yeast homologs (B) and their connection to diseases (C).

(D and E) Venn diagrams showing the distribution of the 189 genes identified as human pre-rRNA processing factors (depletion leads to a >2.5-fold change of at least one pre-RNA species) according to its involvement in early pre-rRNA processing (cleavage at sites 01, A0, and 1), the synthesis of the small (pre-40S) or the large (pre-60S) subunits (D), and functional conservation between 113 human genes and their yeast homologs (E). See also Figure S2 and Tables S2–S6, S9, and S10.

steps since they occur in the nucleolus. Approximately 73% (83 genes) of the human proteins have a function similar to that of their yeast homolog, while the rest have either additional (13.5%) or alternative (13.5%) functions (Figure 2E and Table S6). These observations clearly indicate that ribosome synthesis is far more complex in mammals than was anticipated based on yeast models.

Identification of Human Pre-rRNA Processing Factors

We selected 11 human genes without an obvious yeast homolog and characterized their involvement in pre-rRNA processing in more detail (Figure S3A and Supplemental Experimental Procedures). They are presented in Figure S3A from left to right according to their involvement in early-to-late steps of processing. Most of the genes are implicated in disease. *DUSP11*,

Table 1. Human Pre-rRNA Processing Factors Identified in This Work

Class	Phenotype	Number of Genes	Three siRNAs	Two siRNAs
1	47S down, 45S down, 41S down	67	DDX42, EIF2S3, ISG20L2, KRT18, NCL, NO66,[b] POLR1A, POLR1B, PRDX1, SMC5, UBTF, UTP15	ARPC4, BLM, BUB3, C1orf107, C22orf28, CCDC59, CDCA8, CPSF7, CSTF1, CXorf56, DDX24, DDX31, DDX51, DHX35, DHX8, DNAJC8, EEF1G, EIF2AK2, EIF4A3, EMG1, ESF1, EXOSC8, FEN1, FRG1,[b] HNRNPF, HP1BP3, LUC7L2, MBD3, NOSIP, NPM3, NSUN5, PA2G4, PARN, PELP1, PIN4,[a] POLR2E, PRPF19, RBM4B, RCC2, RPP14, RRN3, SENP3, SEPT2,[b] SERBP1, SFRS3, SNRNP200,[b] TCOF1, TLE1,[b] TOP2A, TTF1,[b] TUFM, TWISTNB, UBE2I, ZFC3H1, ZNF638
2	47S up, 34S up, 30S up	51	CIRH1A, DDB1, DDX41, DUSP11, EXOSC6, FBL, HNRNPC, LSM6, NGDN, NOL6, NOP14, NOP56, PLRG1, PWP2, RRP9, RUVBL1, TBL3, XRN2	AATF, ABT1, BMS1, CDC5L, DDX10, DDX47, DDX49, DNTTIP2, FCF1, HEATR1, HNRNPU, IMP3, IMP4, KRR1, MED21, NHP2L1, NOC4L, NOL10, NOL7, NOM1, NOP58, RCL1,[b] RIOK3, RPS11, SF3B14, SRFBP1, UTP11L, UTP18, UTP20, WDR3, WDR36, WDR43, ZNHIT6
3	47S up, 45S up, 41S up	4	DDX1[a]	EIF2S2, GSTCD,[a] RBM19
4	41S up, 30S down, 21S down, 18S-E up, 12S down	22	BOP1, BRIX1, CSNK1E, GTPBP4, MAK16, NOL9, RRP1, RRP15, RSL1D1, WDR74	CEBPZ, DDX27, EBNA1BP2, EEF1A1, FTSJ2, MKI67IP NOC2L, NOP16, NSA2, PCNA, PES1, PRKDC[b]
5	34S up, 26S down, 18S-E down	7	PRPF8	DHX33, HNRNPL, POLR2H, RBBP4, TOP1, WDR75
6	26S up	8	DKC1, PNO1, SKIV2L, SKIV2L2	ARPC1A,[b] CSNK1D, EXOSC10, EXOSC7
7	21S up, 18S-E down	3	DHX37, RRP12	ZCCHC9
8	21S down, 18S-E down	8	DDX18, MPHOSPH10, WDR46	DDX52, PDCD11, RRP7A, UTP14A, UTP6
9	21S up	6	KRT7,[a] LTV1	APEX1, CDK7,[b] RPP40, RPS3
10	18S-E up	3	WBSCR22	RPF1, TSR2
11	47S up, 32S up	21	CDKN2A, DDX5, GLTSCR2, SPATA5[a]	C4orf43,[b] EFTUD2,[b] EXOSC2,[a] GNL2, HNRNPD, MYBBP1A, NCAPG2,[b] NPM1,[b] PAK1IP1,[b] PPIB, RRS1,[a] SDAD1, SF3A3,[b] SNRPD2,[a] SRPK1, SUV39H1,[b] THYN1[b]
12	12S up	3	EXOSC5	MPHOSPH6, RING1
13	miscellaneous	83	FARSB, ILF3,[b] KIF2C,[b] KPNA3,[a] LAS1L, MRE11A, RBM34,[a] RFC4,[b] TGS1,[a] UTP14C,[a] XPO1	ABCF2,[b] ACTG1,[b] BCAS2, BCCIP,[b] C18orf21,[b] C20orf132,[b] C8orf59,[a] C9orf114,[b] CBX3,[b] CCAR1,[b] CCT2,[b] CDK9,[a] CENPB,[b] COIL,[b] CSNK2A1,[b] DDX54,[b] DEK,[b] DHX15,[a] DNAJC21,[b] DOM3Z,[b] DYRK1B,[b] EEF1A2, EFTUD1,[b] EIF5A,[a] EWSR1, EXOSC1,[b] FABP5,[b] FAM120B,[b] FAM98B,[a] FLNA,[b] FTSJ3,[b] GRSF1,[b] GTPBP5,[a] HMGN4,[b] HNRNPR,[b] IFI16,[b] KRI1,[b] LSG1,[a] MDN1,[a] MRTO4,[a] NAT10,[b] NHP2,[b] NKRF,[a] NOB1,[a] NOC3L,[b] NSUN2,[b] PHF6,[a] PINX1, PPAN, PRPF3,[b] RFC3,[b] RNF40,[b] RPP38,[a] RPSA,[b] RTCD1,[b] RUVBL2, SETX,[b] SFRS1,[b] SFRS5,[b] SIRT7, SPTY2D1,[b] SUB1,[b] TCEB3,[a] TCERG1,[b] TOPBP1,[b] TRMT112,[b] TRMT1L, TRMT6,[b] TSR1,[b] VRK1,[b] WDR12,[b] ZFP106[a]

The table indicates whether two or three siRNAs generated the same or highly similar pre-rRNA profiles. Unless stated otherwise, there is a reduction or accumulation of >2.5-fold of at least one pre-rRNA species tested.
[a]Reduction or accumulation of >2-fold.
[b]Reduction or accumulation of >1.5-fold.

encoding a p53-regulated nuclear RNA-binding dual specificity phosphatase, and *SF3B14* were recently studied in the context of chronic inflammatory disease (Caprara et al., 2009; Deshpande et al., 1999; Häsler et al., 2011; Yuan et al., 1998). *NOL7* is a cervical carcinoma biomarker (Hasina et al., 2006; Huang et al., 2012). *THYN1* has been linked to the Jacobsen haploinsufficiency syndrome (Ji et al., 2010). *NOP16* is a c-Myc-regulated breast cancer marker (Butt et al., 2008). *SRFBP1* is implicated in

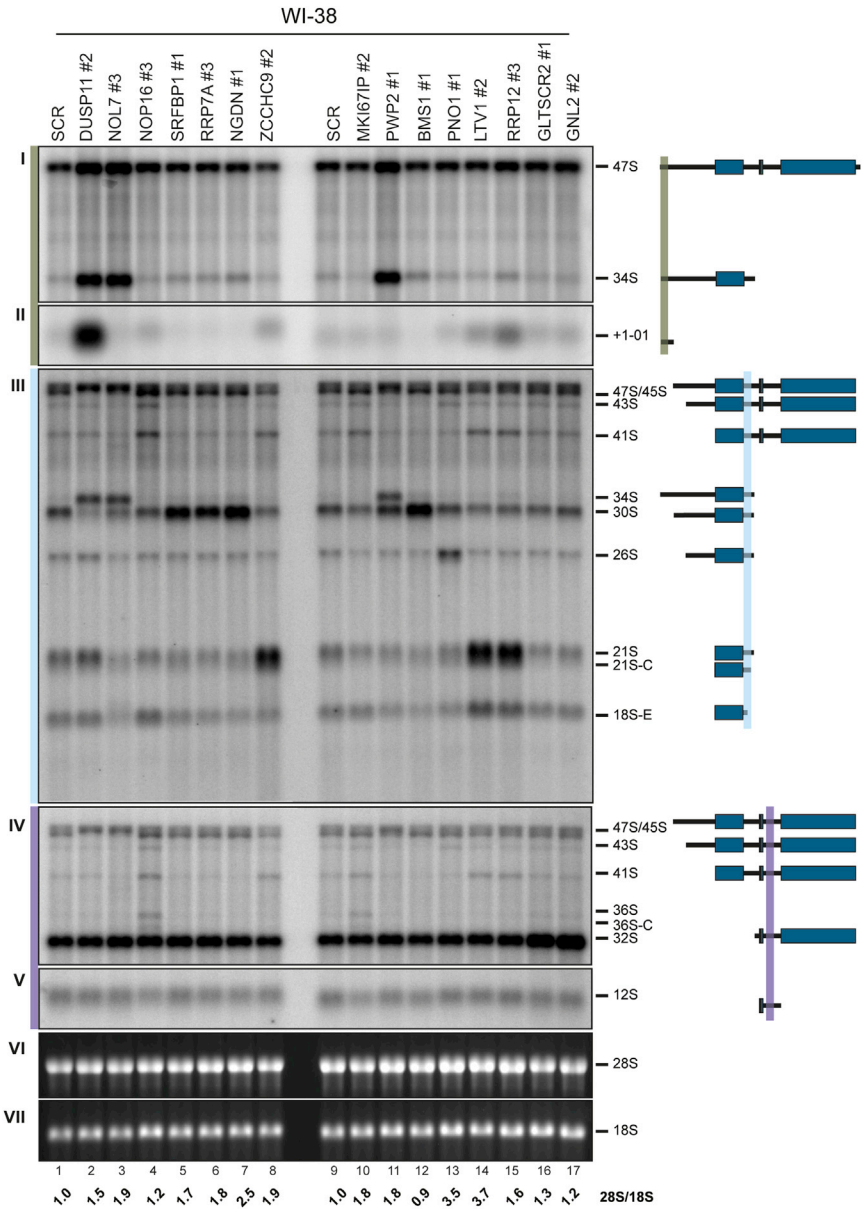

Figure 3. Characterization of Pre-rRNA Processing in Primary Lung Fibroblasts of Seven Human Genes without a Yeast Homolog and Eight Human Genes with a Yeast Homolog Involved in Ribosome Assembly

Analysis of pre-rRNA processing by northern blotting. Total RNA was extracted from WI-38 cells treated for 3 days with a siRNA specific to the target gene, and 2.5 μg were separated by denaturing agarose gel electrophoresis and hybridized with probes (see Figure 1B and Table S8). SCR siRNA was used as a control (lanes 1 and 9). A schematic of the pre-rRNAs detected is shown. Sections I and II, 5′ ETS probe; section III, ITS1 probe; sections IV and V, ITS2 probe. Sections VI and VII show the mature rRNAs on an ethidium bromide-stained gel. The 28S/18S ratio was calculated from Agilent electropherograms. The siRNA sequences (#1 to #3) are listed in Table S7. The 36S and 36S-C precursors (section IV, lanes 4 and 10), corresponding to 5′ extended forms of 32S pre-rRNAs, were unambiguously identified with oligonucleotide LD2655 (specific to sequences between cleavage sites E and 2, data not shown). See also Figure S3.

cardiac cellular metabolism and aging (Zhang et al., 2008; Zhang et al., 2004). *RRP7A* and *SF3B14* are involved in mammalian blastocyst formation and embryo preimplantation (Maserati et al., 2012). *NGDN* is a colon cancer-associated gene (Park et al., 2011). *SFRS3* is proto-oncogene and cancer biomarker diagnostic of early tumorigenesis stages (Jia et al., 2010). Finally, ZCCHC9 is a nuclear protein with weak homology to the RNA exosome cofactors Air1 and Air2 (Sanudo et al., 2011). No information was available on *C8orf59*. In addition to establishing the effects of the depletion of these 11 proteins on pre-rRNA processing, we tested whether any is essential for the maintenance of nucleolar structure and found that none are required (Figure S4 and data not shown).

As further proof of concept, we show the detailed characterization of 39 human genes with yeast processing factor homologs, presented in Figures S3B and S3C from left to right according to their involvement in early-to-late processing steps.

Pre-rRNA Processing Phenotypes Are Conserved in Different Cell Types and Are Not p53 Dependent

We were interested to know whether the pre-rRNA processing phenotypes observed in HeLa cells are conserved in other cell types. We repeated our analysis in primary human fibroblasts (WI-38), testing seven genes without a yeast homolog (*DUSP11*, *NOL7*, *NOP16*, *SRFBP1*, *RRP7A*, *NGDN*, and *ZCCHC9*), eight with a yeast ortholog involved in ribosome synthesis (*MKI67IP*, *PWP2*, *BMS1*, *PNO1*, *LTV1*, *RRP12*, *GLTSCR2*, and *GNL2*), and six RNA exosome subunits and cofactors (Figures 3 and S6B). WI-38 and HeLa cells exhibit similar pre-rRNA processing phenotypes (compare Figures 3 and S3).

A nucleolar p53-dependent tumor surveillance pathway has been described in which insults to ribosome assembly lead to the capture and titration of HDM2 by free unassembled ribosomal components, causing p53 stabilization, G1 cell-cycle arrest, and eventually, cell death (Chakraborty et al., 2011). To clarify whether or not processing defects are the consequence of nucleolar surveillance, the same 21 genes were disrupted in paired human colon carcinoma cell lines (HCT116 $p53^{+/+}$ producing p53; HCT116 $p53^{-/-}$, no p53), and pre-rRNA profiles were compared (Figures 4 and S6B). Pre-rRNA processing defects observed in HCT116 in the presence or in the absence of

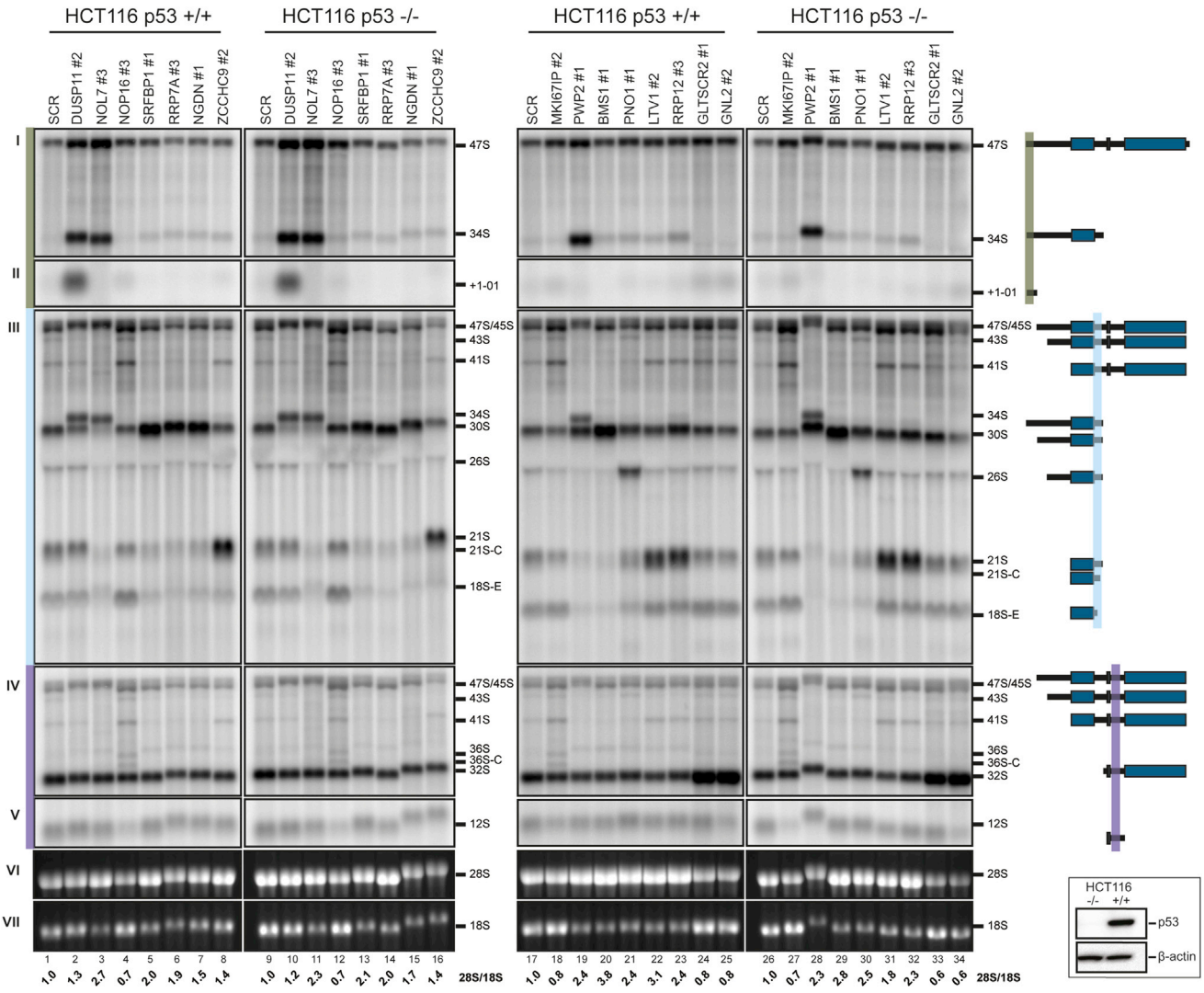

Figure 4. The Pre-rRNA Processing Phenotypes of 15 Representative Genes Are Not p53 Dependent

Analysis of pre-rRNA processing by northern blotting. Total RNA was extracted from HCT116 cells (either expressing p53 or not) treated for 3 days with a siRNA specific to the target gene, and 5 μg were separated by denaturing agarose gel electrophoresis and hybridized with probes (see Figure 1B and Table S8). SCR siRNA was used as a control (lanes 1, 9, 17, and 26). A schematic of the pre-rRNAs detected is provided. Sections I and II, 5′ ETS probe; section III, ITS1 probe; sections IV and V, ITS2 probe. Sections VI and VII show the mature rRNAs on an ethidium bromide-stained gel. The 28S/18S ratio was calculated from Agilent electropherograms. The siRNA sequences (#1 to #3) are listed in Table S7. The western blot (inset) shows the p53 status of the two cell lines used (β-actin was used as a loading control). See also Figure S4.

p53 are virtually identical indicating these processing inhibitions are not p53-dependent. Importantly, this demonstrates the observed phenotypes are not due to the activation of a p53-dependent nucleolar tumor surveillance pathway, known as the ''nucleolar stress'' response. We also conclude the phenotypes reported in WI-38, HeLa and HCT116 are highly conserved.

A detailed description of the processing defects for the set of representative genes is provided in the Supplemental Experimental Procedures. Interestingly, extended forms of 32S (36S and 36S-C), typically detected in patients with DBA-harboring mutations in *RPL26* (see Figure S3A, section IV, lane 1, and Gazda et al., 2012), accumulate in HCT116 cells lacking NOP16 and MKI67IP (Figure 4, section IV, lanes 4, 12, 18, and 27). Notably, this subtle phenotype is conserved in all cell types tested (HeLa, WI-38, HCT116 $p53^{+/+}$, and HCT116 $p53^{-/-}$; Figures 3, 4, and S3). Both NOP16- and RPL26-depleted HeLa and WI-38 cells accumulate more of the long form than of the short form of 5.8S, possibly as a direct consequence of this ITS1 processing defect (Figure S3A, section VII, lanes 1 and 9, and data not shown).

The Pre-rRNA Processing Defects Are Early Events Preceding Cell-Cycle Arrest and Apoptosis

We established the kinetics of processing inhibitions with respect to other cellular processes, such as cell-cycle defects and apoptosis (Figures 5 and S5). A time course analysis was

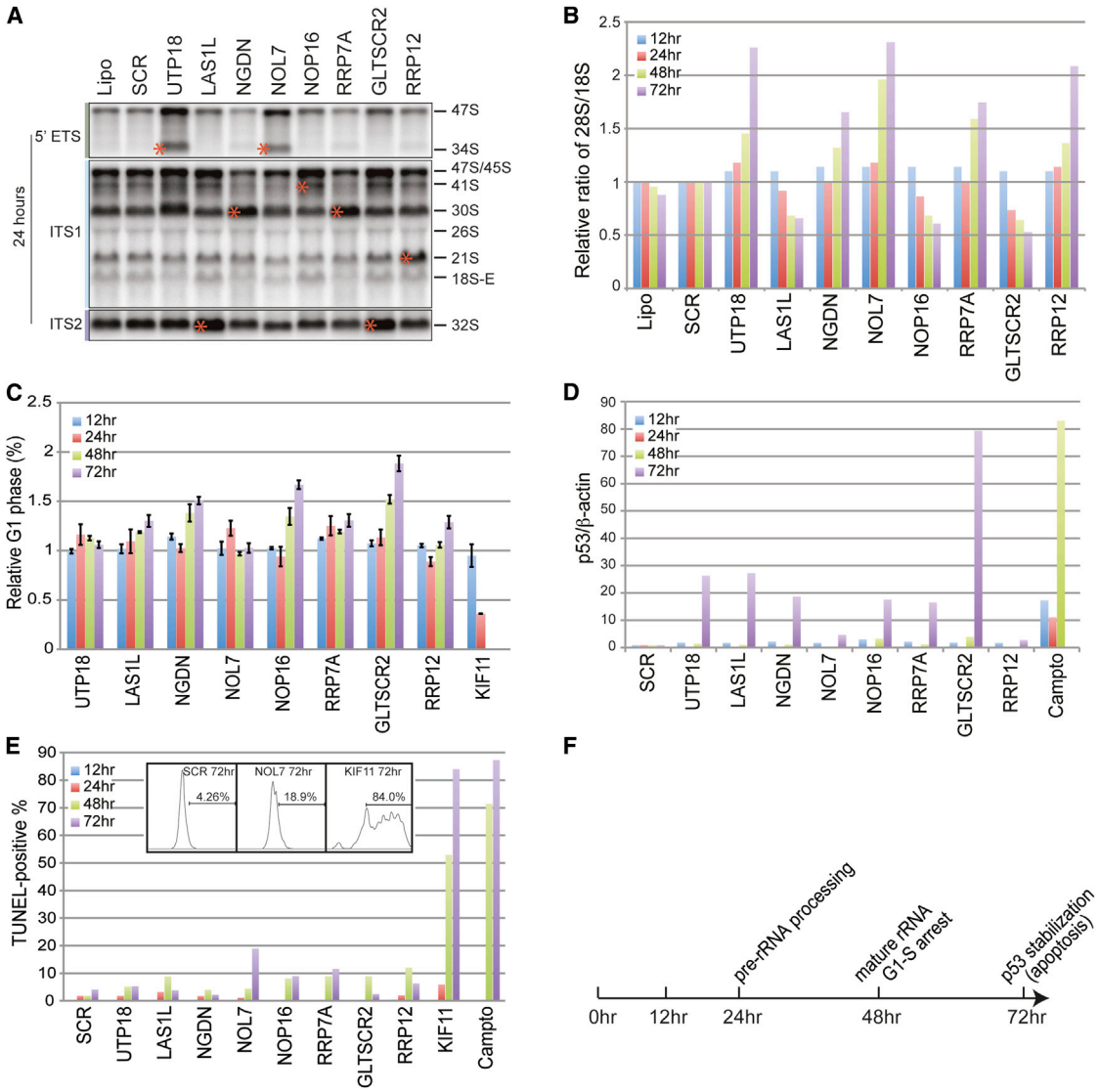

Figure 5. Pre-rRNA Processing Inhibitions Are Early Defects that Precede Cell-Cycle Arrest and Apoptosis

p53-positive HCT116 cells were treated with siRNAs against the indicated genes, and readouts were collected at 12, 24, 48, and 72 hr after depletion. Lipofectamine (Lipo) treatment and SCR siRNA controls were included. Additional controls were cells treated with 1 μM camptothecin (a DNA topoisomerase inhibitor and genotoxic stress inducer) or siRNAs specific to KIF11 (blocks mitosis).

(A) Pre-rRNA processing phenotype established by northern blot hybridization at 24 hr. For each gene, a star highlights a pre-rRNA species diagnostic of the inhibition. See Figure S5 for a complete time course analysis.

(B) Mature rRNA ratio determined by Agilent bioanalyzer capture.

(C) Cell-cycle analysis by FACS. Cells stained with propidium iodide. Signals normalized to SCR. Data are means ± SD of experimental triplicates.

(D) Relative ratio of p53 steady-state accumulation established by quantitative western blot (normalized to β-actin).

(E) Apoptosis level by TUNEL assay. Inset shows representative FACS profiles at 72 hr.

(F) Timeline of the onsets of the different phenotypes analyzed. See also Figure S5.

done in HCT116 $p53^{+/+}$ cells depleted of proteins identified in this study as processing factors (NGDN, NOL7, NOP16, and RRP7A), as well as four with a yeast homolog identified as a processing factor (UTP18, LAS1L, GLTSCR2, and RRP12). We collected readouts at 12, 24, 48, and 72 hr after depletion and analyzed pre-rRNA processing (northern blot; Figures 5A and S5), mature rRNA ratio (Agilent Technologies Bioanalyzer capture; Figure 5B), G1-S cell-cycle arrest (fluorescence-activated cell sorting [FACS] analysis; Figure 5C), relative p53 steady-state accumulation (quantitative western blot; Figure 5D), and apoptosis levels (TUNEL, caspase-3/caspase-7 activation, and Annexin V assays; Figure 5E and data not shown). The data clearly indicate that the processing inhibitions are early defects that are observed as early as 24 hr after depletion for all genes, and even as soon as 12 hr for *UTP18* and *NOL7* (Figure S5), and largely precede the other phenotypes inspected (see

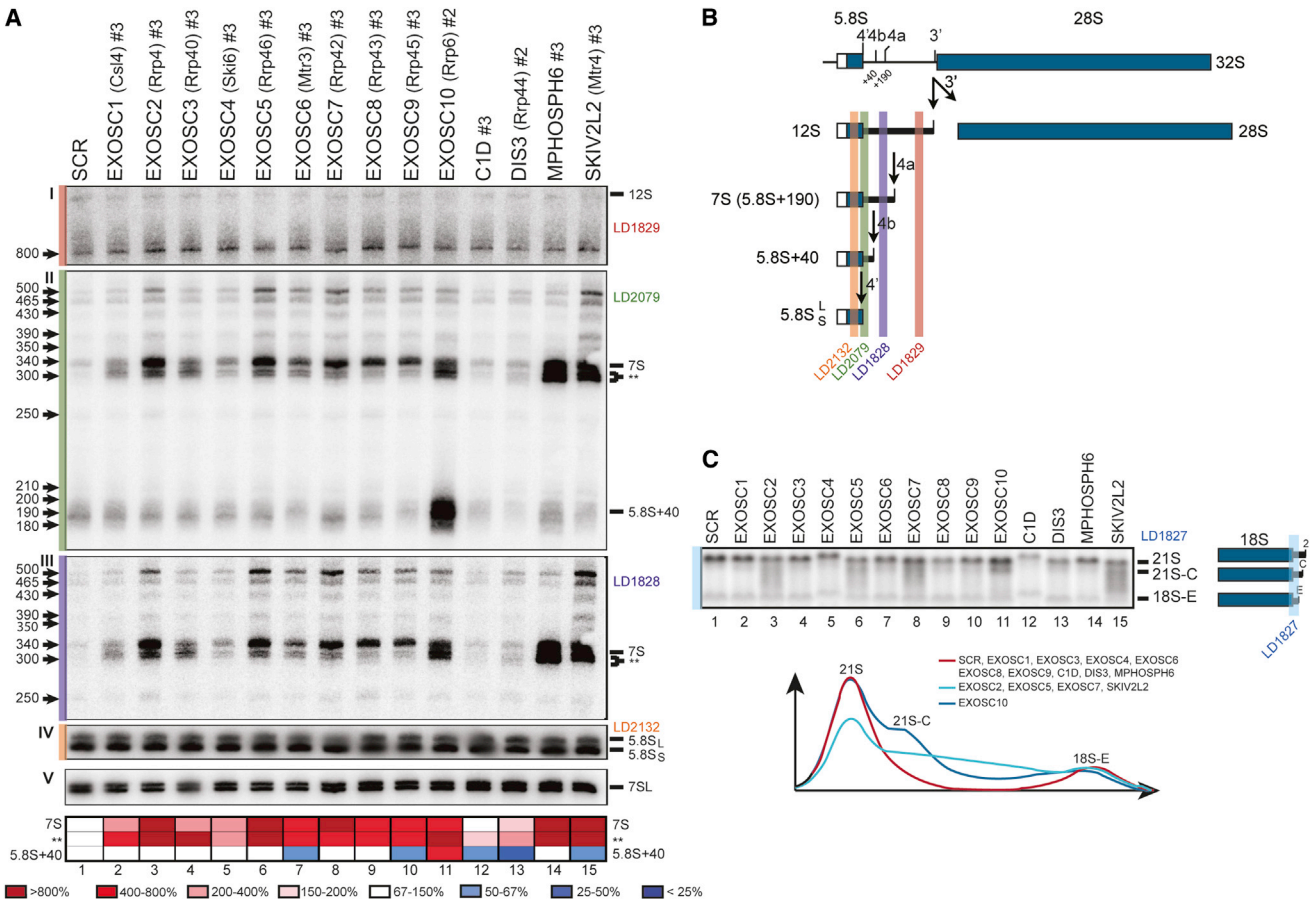

Figure 6. Involvement of Individual Subunits of the Human RNA Exosome in Pre-rRNA Processing of ITS1 and ITS2

(A) Analysis of pre-rRNA processing by northern blotting. Total RNA was extracted from HeLa cells treated for 3 days with a siRNA specific to the target gene, and 5 μg were separated by denaturing acrylamide gel electrophoresis and hybridized with probes specific to ITS2 (LD1828, LD1829, and LD2079; shown in B) or the mature 5.8S rRNA (LD2132). SCR siRNA was used as a control. Section III shows that 5.8S + 40 is detected with probe LD2079, but not LD1828. The 7SL hybridization serves as a loading control. Each band was quantitated with a phosphorimager and converted into a heatmap. Key: see color code. The siRNA sequences (#1 to #3) are listed in Table S7.

(B) Human 5.8S rRNA processing pathway.

(C) Upper panel: high-molecular-weight RNA analysis on denaturing agarose gels of the samples presented in (A). The northern blot was hybridized with LD1827 specific to the 5′ end of ITS1. Lower panel: graphical summary of the effect of exosome subunits on the conversion of 21S to 18S-E. In the absence of EXOSC10, the 21S-C intermediate accumulates, indicating a specific requirement for its conversion into 18S-E. Several other subunits of the exosome (cyan), though not others (red), are also involved in this step to a much lesser extent. See also Figure S6.

timeline; Figure 5F). Indeed, alterations in the mature rRNA ratio and G1-S arrest were only visible at 48 hr, while p53 stabilization was apparent at 72 hr. Apoptosis was barely detected and only after 72 hr (e.g., NOL7; Figure 5E). In conclusion, processing defects largely precede cell-cycle defects and apoptosis in the target genes examined.

Involvement of the Human RNA Exosome in 5.8S and 18S rRNA 3′ End Formation

A surprising observation from this work is that several human gene products have acquired additional or even unique functions in pre-rRNA processing as compared to their yeast homologs (Figure 2E). This is illustrated through the detailed functional characterization of the role of the RNA exosome in ITS1 and ITS2 processing.

In budding yeast, formation of the 3′ end of the 5.8S rRNA, following an initial cleavage in ITS2, involves a complex succession of 3′-5′ exoribonucleolytic digestion by specific RNA exosome subunits (Thomson and Tollervey, 2010 and references therein). We recently provided strong evidence showing that this central biological pathway is evolutionarily conserved and demonstrated highly coordinated communication between processing at the 5′ and 3′ ends of 5.8S rRNA (Schillewaert et al., 2012).

To further characterize ITS2 processing in HeLa cells, we systematically depleted the core exosome subunits and several coactivators (Figure 6). We found a distinctly different requirement for the exosome subunits in trimming 3′-extended 5.8S precursors. The most notable effects were seen on the accumulation of an ~190 nt extended version of 5.8S

rRNA, the 7S pre-rRNA (migrating at 340 nt), and an ~40 nt extended form (migrating at 190 nt) (Figures 6A and 6B). The 7S pre-rRNA strongly accumulated in cells depleted for some (EXOSC2, EXOSC5 to EXOSC10, MPHOSPH6, and SKIV2L2), but oddly, not for other (EXOSC1, EXOSC3, EXOSC4, C1D, and DIS3) exosome components. A doublet migrating just below the 7S was also more abundant only in the absence of EXOSC10, MPHOSPH6, and SKIV2L2 (Figure 6A, sections II and III, lanes 11, 14, and 15). A shorter precursor extended by ~40 nt was only detected in cells lacking EXOSC10 (Figure 6, section II, lane 11). This latter species is likely equivalent to the 5.8S + 30 pre-rRNA that accumulates in yeast cells lacking Rrp6 (yeast EXOSC10) (Briggs et al., 1998).

To ascertain that the distinctly different requirement of exosome subunits and cofactors is not simply the consequence of differential depletion efficiency, we repeated the analysis on six representative subunits and established the residual protein level by western blotting. Under our depletion conditions, we found that the protein levels of the subunits fell nearly to the detection level, yet the processing phenotypes were indeed markedly different (Figure S6A).

This analysis was repeated on the same representative exosome subunits and cofactors in other cell types (Figure S6B). In HCT116 $p53^{+/+}$ and HCT116 $p53^{-/-}$ the phenotypes were similar to those observed in HeLa cells (Figure S6B), again demonstrating that they are not p53 dependent. In primary human lung fibroblasts (WI-38) and primary human umbilical vein endothelial cells (HUVECs), the effects of depleting exosome subunits on ITS2 processing were milder, but the trends observed in HeLa and HCT116 cells were conserved. In particular, the roles of EXOSC10 and SKIV2L2 in 5.8S + 40 and 7S maturation, respectively, were similar (Figure S6B, lanes 5 and 7).

Recently, we discussed that the 18S-E pre-rRNA, an intermediate in the formation of the 18S rRNA (Rouquette et al., 2005), sometimes appears as a fuzzy band on a gel rather than as a discrete one (Mullineux and Lafontaine, 2012). We speculated that this might be because the 18S-E corresponds to a population of RNAs with heterogeneous 3′ ends resulting from exoribonucleolytic trimming of the 21S pre-rRNA, with the 21S-C representing a major intermediate (Figure S1). Consistent with this idea, in the high-molecular-weight RNA analysis of the exosome subunits, we noted that cells depleted for EXOSC10 significantly accumulated the 21S-C (Figure 6C, lane 11). This was also seen with some (EXOSC2, EXOSC5, EXOSC7), but not all, core RNA exosome subunits and with one of its coactivators (SKIV2L2). The data indicate that, unexpectedly, EXOSC10 is also involved in the final trimming of the 18S rRNA. This is in contrast to the situation described in budding yeast, in which Rrp6 is primarily involved in ITS2 processing to generate the 3′ end of 5.8S rRNA but has no known functions in ITS1 processing (Schillewaert et al., 2012 and references therein). We conclude that while the overall architecture of pre-rRNA processing pathways seems to have been well conserved throughout evolution, budding yeast and human cells have adopted different strategies and *trans*-acting factors to perform unique reactions.

DISCUSSION

The emergence of ribosomopathies calls for a deeper understanding of ribosome synthesis in humans. We tested 625 human nucleolar proteins for effects on pre-rRNA processing, a decisive step in ribosome synthesis. We identified 286 factors involved in ribosome biogenesis and generated an online, fully searchable, and information-rich database (Figures 1 and 2, Table S2, and www.ribogenesis.com). Approximately 38% of the genes tested in our study have been linked to diseases, mainly cancer (Figure 2C and Table S5), clearly pointing at a connection between defective ribosome synthesis and disease. This further enhances the need for more detailed studies on human ribosome biogenesis. A large fraction of the nucleolar proteome (339 factors) examined was not required for pre-rRNA processing, which likely reflects proteins involved in extranucleolar functions (Boisvert et al., 2007).

We examined the involvement of 39 human genes in pre-rRNA processing in greater detail; these genes were selected because their yeast homologs are known assembly factors. Nearly 73% carry out RNA cleavage steps similar to their yeast counterparts (Figures S3B and S3C and Table S6), highlighting the evolutionary conservation of key processing steps across eukaryotes. We also characterized 11 disease-related human genes without yeast homologs and showed that they impact distinct steps in the pre-rRNA processing pathway (Figure S3A). This observation supports the notion that expansion of the primary rRNA transcript (13.3 kb in humans versus 6.7 kb in budding yeast) and subsequent emergence of cleavage sites necessitated the recruitment of additional processing factors to catalyze cleavage reactions. These genes belong to a group of 74 members that had previously eluded identification using homology-based methods. Incidentally, we report that among the human proteins identified, 59 have a yeast homolog that has not been examined for a role in ribosome synthesis. Significantly, these include putative methyltransferases, protein modification enzymes, and structural cellular components, as well as gene products involved in translation, pre-mRNA splicing, or DNA replication. These are all cellular processes recently shown to share highly specific *trans*-acting factors with ribosome synthesis. At the time of our analysis, Trm112 belonged to that group but has since been described as a coactivator of the 18S rRNA methyltransferase Bud23 (Figaro et al., 2012; Sardana and Johnson, 2012), making it likely that additional yeast ribosome assembly factors will emerge from this group of genes in the future.

We analyzed 21 genes in other cell types (WI-38, HUVEC, HCT116), including primary cells; the pre-rRNA processing phenotypes observed in HeLa are globally well conserved (Figures 3, 4, and S6B). We also showed that the processing inhibitions are not p53 dependent, indicating importantly that they are not simply the consequence of the activation of a p53-dependent nucleolar tumor surveillance pathway.

Clearly, the large diversity of pre-rRNA processing phenotypes observed in different cell types is evidence that the proteins described in this work are bona fide ribosomal processing factors. To lend additional support to the idea that the proteins identified here are directly involved in ribosome synthesis, we established the kinetics of pre-rRNA processing defects with

respect to other cellular processes, concluding that the cleavage defects precede cell-cycle arrest and apoptosis by at least 24 hr, and even by 36 hr in some cases (Figure 5).

An important biological insight derived from the analysis of our data set is that while many gene products identified in our screen have functions similar to those of their yeast counterpart, around 27% carry additional or even unique functions in pre-rRNA processing (Figure 2E and Table S6). This conclusion will surely impact the manner in which ribosome biogenesis is studied, as it demonstrates that molecular studies of ribosomopathies in the yeast model is no longer sufficient and that the focus must be directed to human cell lines to achieve therapeutic advances. As an example of this, we provided the detailed analysis of the RNA exosome in the processing of the internal transcribed spacers. We demonstrated that the exosome-dependent processing of ITS2 is conserved in different cell types and independent of p53 (Figure S6B). We also showed that the human RNA exosome is involved not only in ITS2 processing, similar to yeast, but also in ITS1 maturation (Figure 6). The involvement of ZCCHC9, the putative homolog of the exosome cofactor Air1/Air2, in the maturation of the 21S pre-rRNA further strengthens the case for the exosome having a function in ITS1 processing in humans (Figures 3, 4, and S3A). The role of the human RNA exosome in ITS1 processing received additional experimental support in a recent independent study (Sloan et al., 2013).

Many genes identified as pre-rRNA processing factors are connected with disease, particularly cancer. Defects in ribosome synthesis can alter ribosome quantity and quality, which immediately impact translation. There is mounting evidence for intimate connections between deregulation of translational control and oncogenic pathways promoting cellular transformation and tumor development (Ruggero, 2013). In the context of ribosome biogenesis, a reduction in functional ribosomes affects the overall protein synthesis capacity of a cell. This clearly poses significant physiological consequences in cell differentiation pathways (e.g., hematopoiesis) at specific steps where the demand in active ribosomes is likely to be especially high (translational bottleneck). The different facets of ribosome biogenesis are highly integrated such that changes in processing kinetics could readily influence rRNA modification patterns. Alterations in ribosome quality (e.g., missing or differentially modified components) also impact the reprogramming of the translational landscape of a cell, with cell- and/or tissue-context-specific pathophysiological consequences (Bellodi et al., 2013; Higa-Nakamine et al., 2012). In particular, rRNA modification has been shown to impact the translation of specific internal ribosome entry site (IRES)-containing mRNAs (Basu et al., 2011; Belin et al., 2009; Jack et al., 2011), which include key tumor suppressors such as p53.

It is also worth noting that in addition to the RNA species, which were systematically investigated for all the genes tested, we identified aberrant rRNA fragments (see www.ribogenesis.com for details). For example, we found that depletion of several late pre-40S assembly factors, such as DIMT1L, DHX37, TSR1, and WBSCR22, led to the accumulation of truncated forms of the 18S-E precursor. This points to a role for these factors in quality control mechanisms, which will require further investigation.

In conclusion, we suggest that despite global conservation in pre-rRNA processing pathways, pre-rRNA intermediates, and processing factors between ancient and modern eukaryotes, plasticity exists and mammals have evolved and adapted distinct cleavage strategies, partially based on the components initially present in deeply rooted eukaryotes.

We hope our database will serve as a key reference data set and fundamental resource to the scientific community, providing useful insights into human disease research and triggering dedicated studies on specific human genes with a ribosome synthesis perspective. Moreover, we have provided powerful evidence showing that pre-rRNA processing is far more complex in humans than previously assumed, created a valuable resource for those investigating ribosomopathies, and identified potentially important biomarkers for malfunctions in ribosome synthesis.

EXPERIMENTAL PROCEDURES

Cell Culture

Cells were grown at 37°C in a humidified incubator with 5% CO_2 in the following media: HeLa (NIH AIDS REF-153), Dulbecco's modified Eagle's medium (DMEM; Sigma D6429)/10% fetal bovine serum (FBS; A&E Scientific); WI-38 cells (ATCC CCL-75), minimal essential medium (MEM; ATCC, 30-2003)/10% FBS; HUVEC (ATCC PCS-100-010), Medium 200 (Life Technologies, M-200-500), supplemented with Low Serum Growth Supplement (LSGS; Life Technologies, S-003-10); and HCT116 (ATCC CCL-247), McCoy's 5A (modified) medium (Sigma)/10% FBS. All media were supplemented with 50 U/ml penicillin and 50 μg/ml streptomycin (Life Technologies).

siRNA Inactivation and Total RNA Extraction

All siRNA were purchased from Life Technologies (Silencer Select siRNA). Three unique silencers were designed for each target gene and used in three individual reactions (Table S7). HeLa, WI-38, and HCT116 cells were reverse transfected as follows: 1.5 μl of 20 μM siRNA (10 nM final) and 4 μl Lipofectamine RNAiMAX (Life Technologies) were mixed with 500 μl of Opti-MEM (GIBCO) in each well of a 6-well plate. After a 20 min incubation at room temperature, 1.5×10^5 cells, resuspended in 2.5 ml of medium without antibiotics, were seeded in each well. Inactivations were carried out for 72 hr prior to total RNA extraction. Negative controls were transfected either with a scrambled (SCR) siRNA (4390844) or without siRNA (mock transfected), with similar results. A calibration set (described in Figure 1) was included in each batch of siRNA-mediated depletions. HUVECs were reverse transfected (same protocol) using 2×10^5 cells per well in a 6-well plate, respectively. siRNA sequences for the calibration set (UTP18#1, RPS3#3, RPS11#1, NOL9#1) are listed in Table S7. Total RNA was extracted using the TRI Reagent (Life Technologies) according to the manufacturer's protocol and analyzed by northern blotting and/or qPCR, as described below.

RNA Electrophoresis

For analysis of high-molecular-weight species, 5 μg of total RNA were resolved on agarose denaturing gels (6% formaldehyde/1.2% agarose in HEPES-EDTA buffer). For low-resolution analysis (screening gels), gels were migrated for 4 hr at 75 V. For higher resolution (Figures 1C, 3, 4, 6, and S3), electrophoresis was carried out for 16 hr at 60 V. For the analysis of the low-molecular-weight RNA species, either 1 μg (for the 7SL loading control) or 5 μg (for the exosome subunit analysis) of total RNA were separated on denaturing acrylamide gels (8% acrylamide-bisacrylamide 19:1/8 M urea in Tris-borate-EDTA buffer [TBE]) for 4 hr at 350 V.

Northern Blotting

Agarose gels were transferred by capillarity overnight in 10× saline sodium citrate (SSC) and acrylamide gels by electrotransfer in 0.5× TBE on nylon membranes (GE Healthcare). Membranes were prehybridized for 1 hr at 65°C in

50% formamide, 5× SSPE, 5× Denhardt's solution, 1% w/v SDS, 200 μg/ml fish sperm DNA solution (Roche). The ^{32}P-labeled oligonucleotide probe was added and incubated for 1 hr at 65°C and then overnight at 37°C. Sequences of the probes are described in Table S8.

SUPPLEMENTAL INFORMATION

Supplemental Information includes Supplemental Experimental Procedures, six figures, and ten tables and can be found with this article online at http://dx.doi.org/10.1016/j.molcel.2013.08.011.

ACKNOWLEDGMENTS

We acknowledge support from the following: Drs. Catherine Denicourt (University of Texas Health Science Center) for providing the HCT116 cell lines, Nick Watkins (University of Newcastle) for providing antibodies to specific exosome subunits, Danièle Hernandez-Verdun (Institut Jacques Monod, Université Paris Diderot-Paris 7) for cell lines, Benoit Van Driessche (ULB, Molecular Virology) for valuable advice in human cell culture, Nicolas Simonis (ULB, Bioinformatics of Genomes and Networks) for assistance with the use of the clustering software R, Vincent Duheron (ULB, Biology of the Nucleus) for help with FACS analysis, and Emilien Nicolas (ULB, CMMI) for critical reading. We also acknowledge the insightful comments and suggestions of anonymous reviewers. The lab of D.L.J.L. is funded by the F.R.S./FNRS and FEDER (through involvement in the CMMI).

Received: February 18, 2013
Revised: June 6, 2013
Accepted: July 17, 2013
Published: August 22, 2013

REFERENCES

Ahmad, Y., Boisvert, F.M., Gregor, P., Cobley, A., and Lamond, A.I. (2009). NOPdb: Nucleolar Proteome Database—2008 update. Nucleic Acids Res. *37*(Database issue), D181–D184.

Andersen, J.S., Lyon, C.E., Fox, A.H., Leung, A.K., Lam, Y.W., Steen, H., Mann, M., and Lamond, A.I. (2002). Directed proteomic analysis of the human nucleolus. Curr. Biol. *12*, 1–11.

Andersen, J.S., Lam, Y.W., Leung, A.K., Ong, S.E., Lyon, C.E., Lamond, A.I., and Mann, M. (2005). Nucleolar proteome dynamics. Nature *433*, 77–83.

Ashraf, N., Zino, S., Macintyre, A., Kingsmore, D., Payne, A.P., George, W.D., and Shiels, P.G. (2006). Altered sirtuin expression is associated with node-positive breast cancer. Br. J. Cancer *95*, 1056–1061.

Basu, A., Das, P., Chaudhuri, S., Bevilacqua, E., Andrews, J., Barik, S., Hatzoglou, M., Komar, A.A., and Mazumder, B. (2011). Requirement of rRNA methylation for 80S ribosome assembly on a cohort of cellular internal ribosome entry sites. Mol. Cell. Biol. *31*, 4482–4499.

Belin, S., Beghin, A., Solano-Gonzàlez, E., Bezin, L., Brunet-Manquat, S., Textoris, J., Prats, A.C., Mertani, H.C., Dumontet, C., and Diaz, J.J. (2009). Dysregulation of ribosome biogenesis and translational capacity is associated with tumor progression of human breast cancer cells. PLoS ONE *4*, e7147.

Bellodi, C., McMahon, M., Contreras, A., Juliano, D., Kopmar, N., Nakamura, T., Maltby, D., Burlingame, A., Savage, S.A., Shimamura, A., and Ruggero, D. (2013). H/ACA small RNA dysfunctions in disease reveal key roles for noncoding RNA modifications in hematopoietic stem cell differentiation. Cell Rep *3*, 1493–1502.

Boisvert, F.M., van Koningsbruggen, S., Navascués, J., and Lamond, A.I. (2007). The multifunctional nucleolus. Nat. Rev. Mol. Cell Biol. *8*, 574–585.

Bolze, A., Mahlaoui, N., Byun, M., Turner, B., Trede, N., Ellis, S.R., Abhyankar, A., Itan, Y., Patin, E., Brebner, S., et al. (2013). Ribosomal protein SA haploinsufficiency in humans with isolated congenital asplenia. Science *340*, 976–978.

Boulon, S., Westman, B.J., Hutten, S., Boisvert, F.M., and Lamond, A.I. (2010). The nucleolus under stress. Mol. Cell *40*, 216–227.

Briggs, M.W., Burkard, K.T., and Butler, J.S. (1998). Rrp6p, the yeast homologue of the human PM-Scl 100-kDa autoantigen, is essential for efficient 5.8 S rRNA 3′ end formation. J. Biol. Chem. *273*, 13255–13263.

Butt, A.J., Sergio, C.M., Inman, C.K., Anderson, L.R., McNeil, C.M., Russell, A.J., Nousch, M., Preiss, T., Biankin, A.V., Sutherland, R.L., and Musgrove, E.A. (2008). The estrogen and c-Myc target gene HSPC111 is over-expressed in breast cancer and associated with poor patient outcome. Breast Cancer Res. *10*, R28.

Caprara, G., Zamponi, R., Melixetian, M., and Helin, K. (2009). Isolation and characterization of DUSP11, a novel p53 target gene. J. Cell. Mol. Med. *13*(8B), 2158–2170.

Chakraborty, A., Uechi, T., and Kenmochi, N. (2011). Guarding the 'translation apparatus': defective ribosome biogenesis and the p53 signaling pathway. Wiley Interdiscip Rev RNA *2*, 507–522.

De Keersmaecker, K., Atak, Z.K., Li, N., Vicente, C., Patchett, S., Girardi, T., Gianfelici, V., Geerdens, E., Clappier, E., Porcu, M., et al. (2013). Exome sequencing identifies mutation in CNOT3 and ribosomal genes RPL5 and RPL10 in T-cell acute lymphoblastic leukemia. Nat. Genet. *45*, 186–190.

Deshpande, T., Takagi, T., Hao, L., Buratowski, S., and Charbonneau, H. (1999). Human PIR1 of the protein-tyrosine phosphatase superfamily has RNA 5′-triphosphatase and diphosphatase activities. J. Biol. Chem. *274*, 16590–16594.

Dimario, P.J. (2004). Cell and molecular biology of nucleolar assembly and disassembly. Int. Rev. Cytol. *239*, 99–178.

Fan, B.J., Wang, D.Y., Cheng, C.Y., Ko, W.C., Lam, S.C., and Pang, C.P. (2009). Different WDR36 mutation pattern in Chinese patients with primary open-angle glaucoma. Mol. Vis. *15*, 646–653.

Farrar, J.E., Vlachos, A., Atsidaftos, E., Carlson-Donohoe, H., Markello, T.C., Arceci, R.J., Ellis, S.R., Lipton, J.M., and Bodine, D.M. (2011). Ribosomal protein gene deletions in Diamond-Blackfan anemia. Blood *118*, 6943–6951.

Figaro, S., Wacheul, L., Schillewaert, S., Graille, M., Huvelle, E., Mongeard, R., Zorbas, C., Lafontaine, D.L.J., and Heurgué-Hamard, V. (2012). Trm112 is required for Bud23-mediated methylation of the 18S rRNA at position G1575. Mol. Cell. Biol. *32*, 2254–2267.

Gazda, H.T., Preti, M., Sheen, M.R., O'Donohue, M.F., Vlachos, A., Davies, S.M., Kattamis, A., Doherty, L., Landowski, M., Buros, C., et al. (2012). Frameshift mutation in p53 regulator RPL26 is associated with multiple physical abnormalities and a specific pre-ribosomal RNA processing defect in diamond-blackfan anemia. Hum. Mutat. *33*, 1037–1044.

Hasina, R., Pontier, A.L., Fekete, M.J., Martin, L.E., Qi, X.M., Brigaudeau, C., Pramanik, R., Cline, E.I., Coignet, L.J., and Lingen, M.W. (2006). NOL7 is a nucleolar candidate tumor suppressor gene in cervical cancer that modulates the angiogenic phenotype. Oncogene *25*, 588–598.

Häsler, R., Kerick, M., Mah, N., Hultschig, C., Richter, G., Bretz, F., Sina, C., Lehrach, H., Nietfeld, W., Schreiber, S., and Rosenstiel, P. (2011). Alterations of pre-mRNA splicing in human inflammatory bowel disease. Eur. J. Cell Biol. *90*, 603–611.

Heindl, K., and Martinez, J. (2010). Nol9 is a novel polynucleotide 5′-kinase involved in ribosomal RNA processing. EMBO J. *29*, 4161–4171.

Higa-Nakamine, S., Suzuki, T., Uechi, T., Chakraborty, A., Nakajima, Y., Nakamura, M., Hirano, N., Suzuki, T., and Kenmochi, N. (2012). Loss of ribosomal RNA modification causes developmental defects in zebrafish. Nucleic Acids Res. *40*, 391–398.

Hölzel, M., Orban, M., Hochstatter, J., Rohrmoser, M., Harasim, T., Malamoussi, A., Kremmer, E., Längst, G., and Eick, D. (2010). Defects in 18 S or 28 S rRNA processing activate the p53 pathway. J. Biol. Chem. *285*, 6364–6370.

Huang, L., Zheng, M., Zhou, Q.M., Zhang, M.Y., Yu, Y.H., Yun, J.P., and Wang, H.Y. (2012). Identification of a 7-gene signature that predicts relapse and survival for early stage patients with cervical carcinoma. Med. Oncol. *29*, 2911–2918.

Huh, W.K., Falvo, J.V., Gerke, L.C., Carroll, A.S., Howson, R.W., Weissman, J.S., and O'Shea, E.K. (2003). Global analysis of protein localization in budding yeast. Nature *425*, 686–691.

Jack, K., Bellodi, C., Landry, D.M., Niederer, R.O., Meskauskas, A., Musalgaonkar, S., Kopmar, N., Krasnykh, O., Dean, A.M., Thompson, S.R., et al. (2011). rRNA pseudouridylation defects affect ribosomal ligand binding and translational fidelity from yeast to human cells. Mol. Cell *44*, 660–666.

Ji, T., Wu, Y., Wang, H., Wang, J., and Jiang, Y. (2010). Diagnosis and fine mapping of a deletion in distal 11q in two Chinese patients with developmental delay. J. Hum. Genet. *55*, 486–489.

Jia, R., Li, C., McCoy, J.P., Deng, C.X., and Zheng, Z.M. (2010). SRp20 is a proto-oncogene critical for cell proliferation and tumor induction and maintenance. Int. J. Biol. Sci. *6*, 806–826.

Johnson, A.W., and Ellis, S.R. (2011). Of blood, bones, and ribosomes: is Swachman-Diamond syndrome a ribosomopathy? Genes Dev. *25*, 898–900.

Lafontaine, D.L.J. (2010). A 'garbage can' for ribosomes: how eukaryotes degrade their ribosomes. Trends Biochem. Sci. *35*, 267–277.

Lam, Y.W., Evans, V.C., Heesom, K.J., Lamond, A.I., and Matthews, D.A. (2010). Proteomics analysis of the nucleolus in adenovirus-infected cells. Mol. Cell. Proteomics *9*, 117–130.

Maserati, M., Dai, X., Walentuk, M., and Mager, J. (2012). Identification of four genes required for mammalian blastocyst formation. Zygote, 1–9. Published online December 5, 2012. http://dx.doi.org/10.1017/S0967199412000561.

Moore, H.M., Bai, B., Boisvert, F.M., Latonen, L., Rantanen, V., Simpson, J.C., Pepperkok, R., Lamond, A.I., and Laiho, M. (2011). Quantitative proteomics and dynamic imaging of the nucleolus reveal distinct responses to UV and ionizing radiation. Mol. Cell. Proteomics *10*, 009241.

Mullineux, S.T., and Lafontaine, D.L.J. (2012). Mapping the cleavage sites on mammalian pre-rRNAs: where do we stand? Biochimie *94*, 1521–1532.

Narla, A., and Ebert, B.L. (2011). Translational medicine: ribosomopathies. Blood *118*, 4300–4301.

O'Donohue, M.F., Choesmel, V., Faubladier, M., Fichant, G., and Gleizes, P.E. (2010). Functional dichotomy of ribosomal proteins during the synthesis of mammalian 40S ribosomal subunits. J. Cell Biol. *190*, 853–866.

Olson, M.O., and Dundr, M. (2005). The moving parts of the nucleolus. Histochem. Cell Biol. *123*, 203–216.

Ozenne, P., Eymin, B., Brambilla, E., and Gazzeri, S. (2010). The ARF tumor suppressor: structure, functions and status in cancer. Int. J. Cancer *127*, 2239–2247.

Park, J.H., Sihn, C.R., Lee, Y.S., Lee, S.J., and Kim, S.H. (2011). Depletion of Neuroguidin/CANu1 sensitizes human osteosarcoma U2OS cells to doxorubicin. BMB Rep *44*, 46–51.

Pendle, A.F., Clark, G.P., Boon, R., Lewandowska, D., Lam, Y.W., Andersen, J., Mann, M., Lamond, A.I., Brown, J.W., and Shaw, P.J. (2005). Proteomic analysis of the Arabidopsis nucleolus suggests novel nucleolar functions. Mol. Biol. Cell *16*, 260–269.

Perotti, D., De Vecchi, G., Testi, M.A., Lualdi, E., Modena, P., Mondini, P., Ravagnani, F., Collini, P., Di Renzo, F., Spreafico, F., et al. (2004). Germline mutations of the POU6F2 gene in Wilms tumors with loss of heterozygosity on chromosome 7p14. Hum. Mutat. *24*, 400–407.

Phair, R.D., and Misteli, T. (2000). High mobility of proteins in the mammalian cell nucleus. Nature *404*, 604–609.

Rouquette, J., Choesmel, V., and Gleizes, P.E. (2005). Nuclear export and cytoplasmic processing of precursors to the 40S ribosomal subunits in mammalian cells. EMBO J. *24*, 2862–2872.

Ruggero, D. (2013). Translational control in cancer etiology. Cold Spring Harb. Perspect. Biol. *5*, 5.

Ruggero, D., and Pandolfi, P.P. (2003). Does the ribosome translate cancer? Nat. Rev. Cancer *3*, 179–192.

Sanudo, M., Jacko, M., Rammelt, C., Vanacova, S., and Stefl, R. (2011). 1H, 13C, and 15N chemical shift assignments of ZCCHC9. Biomol. NMR Assign. *5*, 19–21.

Sardana, R., and Johnson, A.W. (2012). The methyltransferase adaptor protein Trm112 is involved in biogenesis of both ribosomal subunits. Mol. Biol. Cell *23*, 4313–4322.

Sasaki, M., Kawahara, K., Nishio, M., Mimori, K., Kogo, R., Hamada, K., Itoh, B., Wang, J., Komatsu, Y., Yang, Y.R., et al. (2011). Regulation of the MDM2-P53 pathway and tumor growth by PICT1 via nucleolar RPL11. Nat. Med. *17*, 944–951.

Scherl, A., Couté, Y., Déon, C., Callé, A., Kindbeiter, K., Sanchez, J.C., Greco, A., Hochstrasser, D., and Diaz, J.J. (2002). Functional proteomic analysis of human nucleolus. Mol. Biol. Cell *13*, 4100–4109.

Schillewaert, S., Wacheul, L., Lhomme, F., and Lafontaine, D.L.J. (2012). The evolutionarily conserved protein Las1 is required for pre-rRNA processing at both ends of ITS2. Mol. Cell. Biol. *32*, 430–444.

Sloan, K.E., Mattijssen, S., Lebaron, S., Tollervey, D., Pruijn, G.J., and Watkins, N.J. (2013). Both endonucleolytic and exonucleolytic cleavage mediate ITS1 removal during human ribosomal RNA processing. J. Cell Biol. *200*, 577–588.

Thomson, E., and Tollervey, D. (2010). The final step in 5.8S rRNA processing is cytoplasmic in Saccharomyces cerevisiae. Mol. Cell. Biol. *30*, 976–984.

Yuan, Y., Li, D.M., and Sun, H. (1998). PIR1, a novel phosphatase that exhibits high affinity to RNA. ribonucleoprotein complexes. J. Biol. Chem. *273*, 20347–20353.

Zhang, X., Azhar, G., Zhong, Y., and Wei, J.Y. (2004). Identification of a novel serum response factor cofactor in cardiac gene regulation. J. Biol. Chem. *279*, 55626–55632.

Zhang, X., Azhar, G., Helms, S., Zhong, Y., and Wei, J.Y. (2008). Identification of a subunit of NADH-dehydrogenase as a p49/STRAP-binding protein. BMC Cell Biol. *9*, 8.

Molecular Cell, Volume *51*

Supplemental Information

The Complexity of Human Ribosome Biogenesis Revealed by Systematic Nucleolar Screening of Pre-rRNA Processing Factors

Lionel Tafforeau, Christiane Zorbas, Jean-Louis Langhendries, Sahra-Taylor Mullineux, Vassiliki Stamatopoulou, Romain Mullier, Ludivine Wacheul, and Denis L.J. Lafontaine

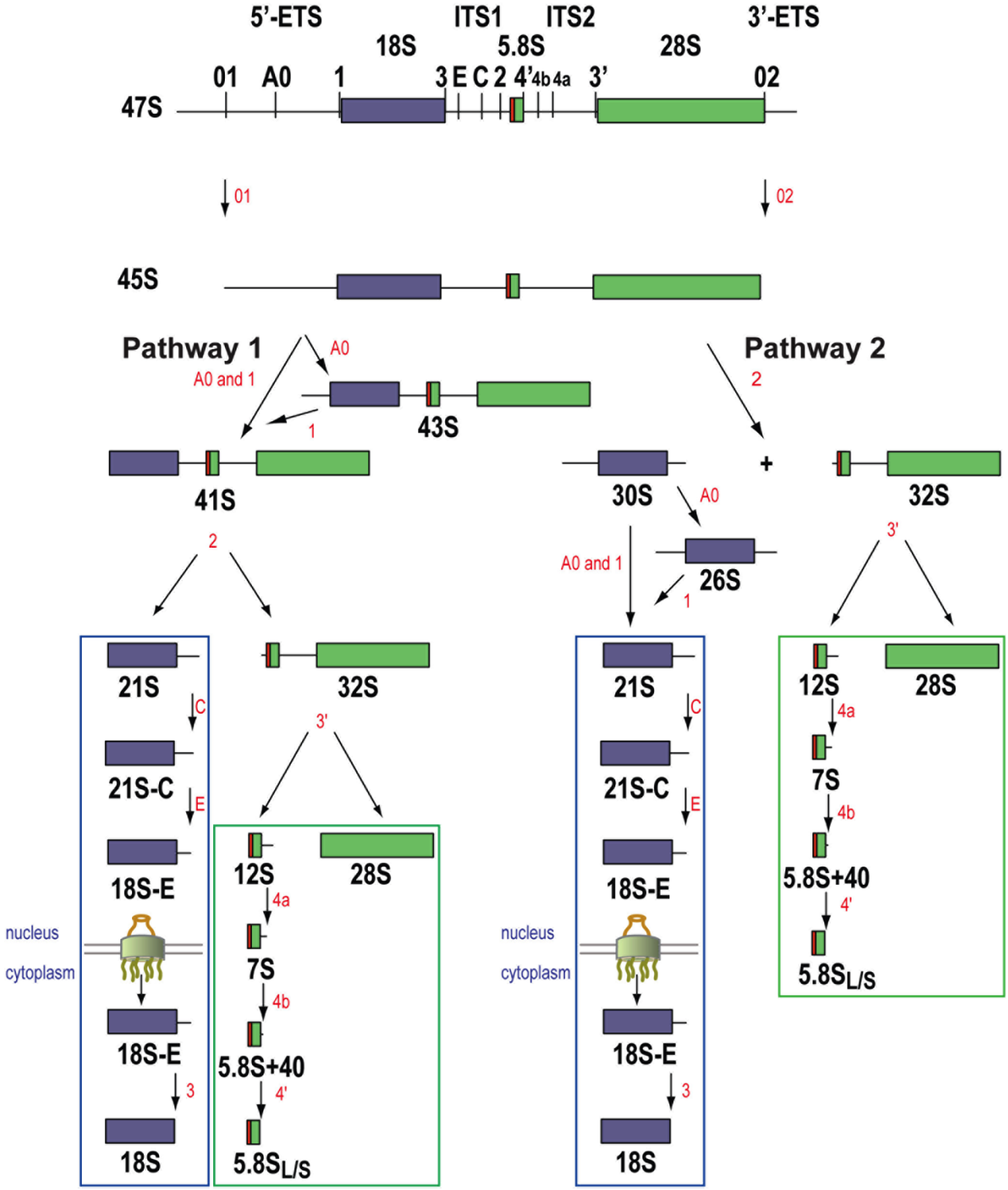
5'-ETS
ITS1
ITS2
3'-ETS
18S
5.8S
28S
01
A0
1
3
E
C
2
4'
4b
4a
3'
02
47S
01
02
45S
Pathway 1
A0
A0 and 1
1
43S
41S
2
21S
C
21S-C
E
18S-E
nucleus
cytoplasm
18S-E
3
18S
32S
3'
12S
28S
4a
7S
4b
5.8S+40
4'
5.8S L/S
Pathway 2
2
+
30S
A0
32S
A0 and 1
26S
1
3'
21S
C
21S-C
E
18S-E
nucleus
cytoplasm
18S-E
3
18S
12S
28S
4a
7S
4b
5.8S+40
4'
5.8S L/S

Figure S1. Pre-rRNA Processing Pathway in Cultured Human Cells, Related to Figure 1

The 18S, 5.8S, and 28S rRNA sequences are flanked by the 5' and 3' ETS, ITS1 and ITS2. The primary transcript (47S) is cleaved at sites 01 and 02, generating the 45S pre-rRNA, which is processed by two alternative pathways. In a minor pathway, site A0, in the 5' ETS, and site 1, at the 5' end of 18S rRNA, are cleaved, yielding the 41S pre-rRNA. The 41S is digested at site 2 within ITS1, separating the RNA precursors destined to become the small and large subunits, the 21S and 32S species, respectively. The 21S is cleaved at site E, producing the 18S-E intermediate, which is then processed at site 3 into the mature 18S rRNA. Maturation of the 21S is a sequential process, and a 21S-C intermediate is detected upon depletion of specific assembly factors (e.g., see RPS3 depletion, Fig 1C). Processing of the 32S within ITS2 generates the 12S and the 28S mature rRNA. The 12S pre-rRNA is successively trimmed to produce the 5.8S rRNA by a series of exoribonucleolytic digestions involving specific subunits of the RNA exosome (Fig 6). In the alternative major pathway, the 45S pre-rRNA is directly cleaved at site 2 in ITS1, prior to cleavage at sites A0 and 1, generating the 30S and 32S species. Processing of the 30S pre-RNA at sites A0 and 1 produces, respectively, the 26S and 21S. In human cells, as in budding yeast, there are two forms, short and long, of 5.8S rRNA (red extension). Synthesis of the 26S results from partial uncoupling of cleavages at sites A0 and 1; when such uncoupling occurs the 43S pre-rRNA can also be observed. Similar branches in the two major pathways are boxed in blue and green.

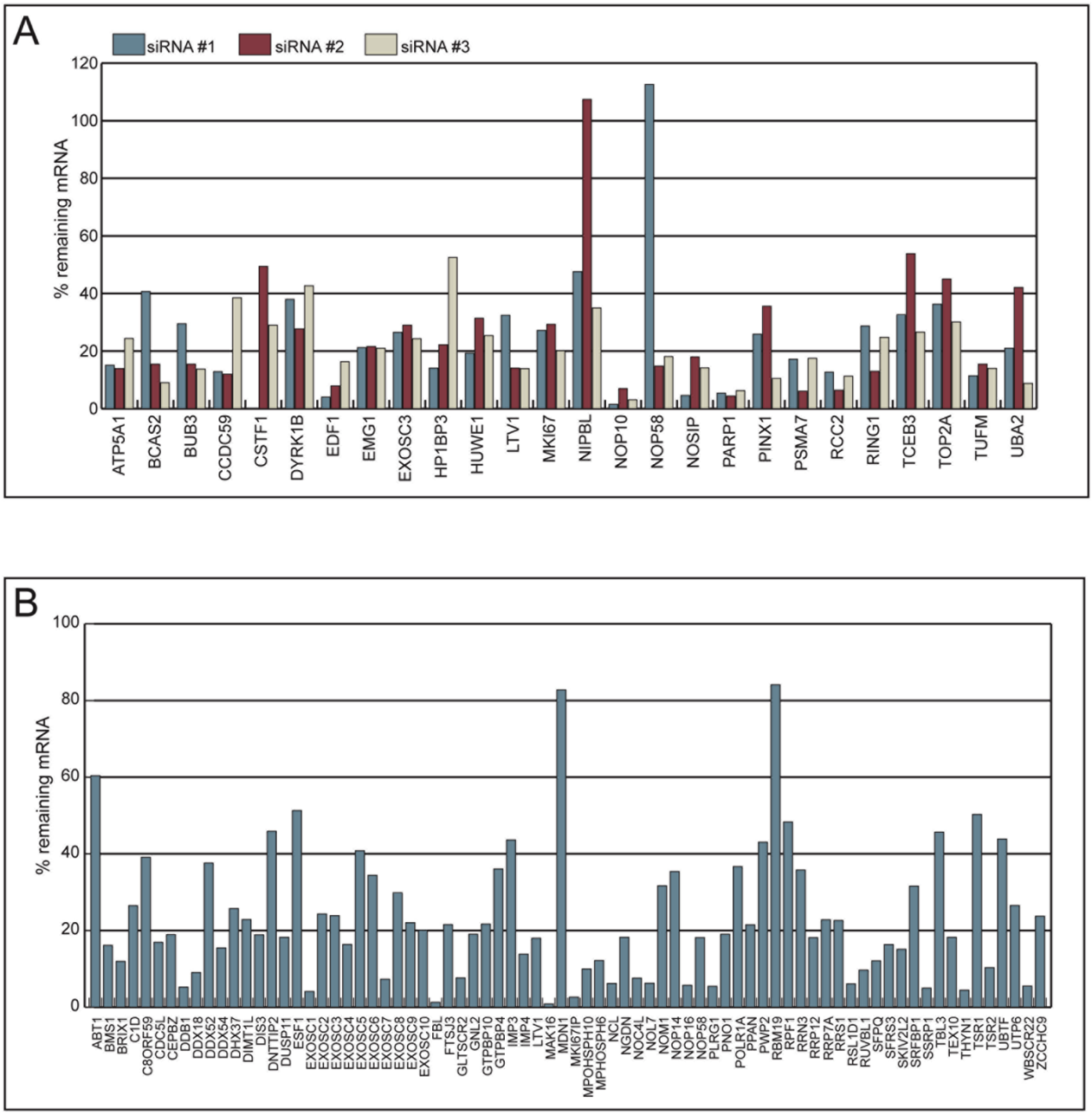

Figure S2. Shotgun qPCR Validation of mRNA Depletion for Randomly Selected Genes, Related to Figure 2

The histograms illustrate the residual level of targeted mRNA (normalized to GAPDH), as assayed by qPCR after a 3 d siRNA-mediated depletion. **A** the efficiency of the three siRNAs was tested for 26 randomly selected genes. **B** the efficiency of one siRNA was tested for 76 randomly selected genes. See also Supplemental Table S9.

A

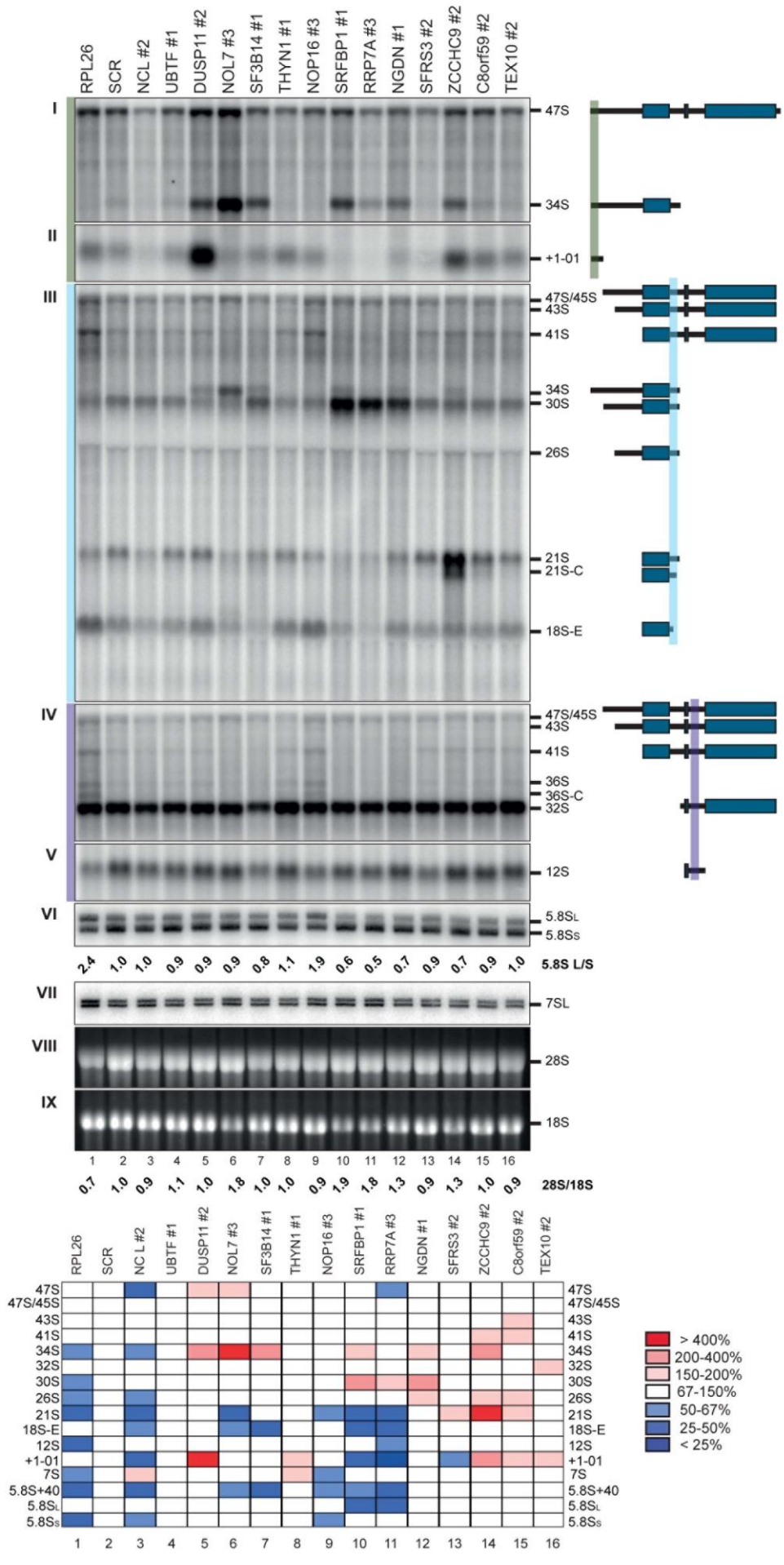
RPL26
SCR
NCL #2
UBTF #1
DUSP11 #2
NOL7 #3
SF3B14 #1
THYN1 #1
NOP16 #3
SRFBP1 #1
RRP7A #3
NGDN #1
SFRS3 #2
ZCCHC9 #2
C8orf59 #2
TEX10 #2
I
47S
34S
II
+1-01
III
47S/45S
43S
41S
34S
30S
26S
21S
21S-C
18S-E
IV
47S/45S
43S
41S
36S
36S-C
32S
V
12S
VI
5.8SL
5.8Ss
2.4 1.0 1.0 0.9 0.9 0.9 0.8 1.1 1.9 0.6 0.5 0.7 0.9 0.7 0.9 1.0
5.8S L/S
VII
7SL
VIII
28S
IX
18S
1 2 3 4 5 6 7 8 9 10 11 12 13 14 15 16
0.7 1.0 0.9 1.1 1.0 1.8 1.0 1.0 0.9 1.9 1.8 1.3 0.9 1.3 1.0 0.9
28S/18S
RPL26
SCR
NC L #2
UBTF #1
DUSP11 #2
NOL7 #3
SF3B14 #1
THYN1 #1
NOP16 #3
SRFBP1 #1
RRP7A #3
NGDN #1
SFRS3 #2
ZCCHC9 #2
C8orf59 #2
TEX10 #2
47S
47S/45S
43S
41S
34S
32S
30S
26S
21S
18S-E
12S
+1-01
7S
5.8S+40
5.8SL
5.8Ss
1 2 3 4 5 6 7 8 9 10 11 12 13 14 15 16
> 400%
200-400%
150-200%
67-150%
50-67%
25-50%
< 25%

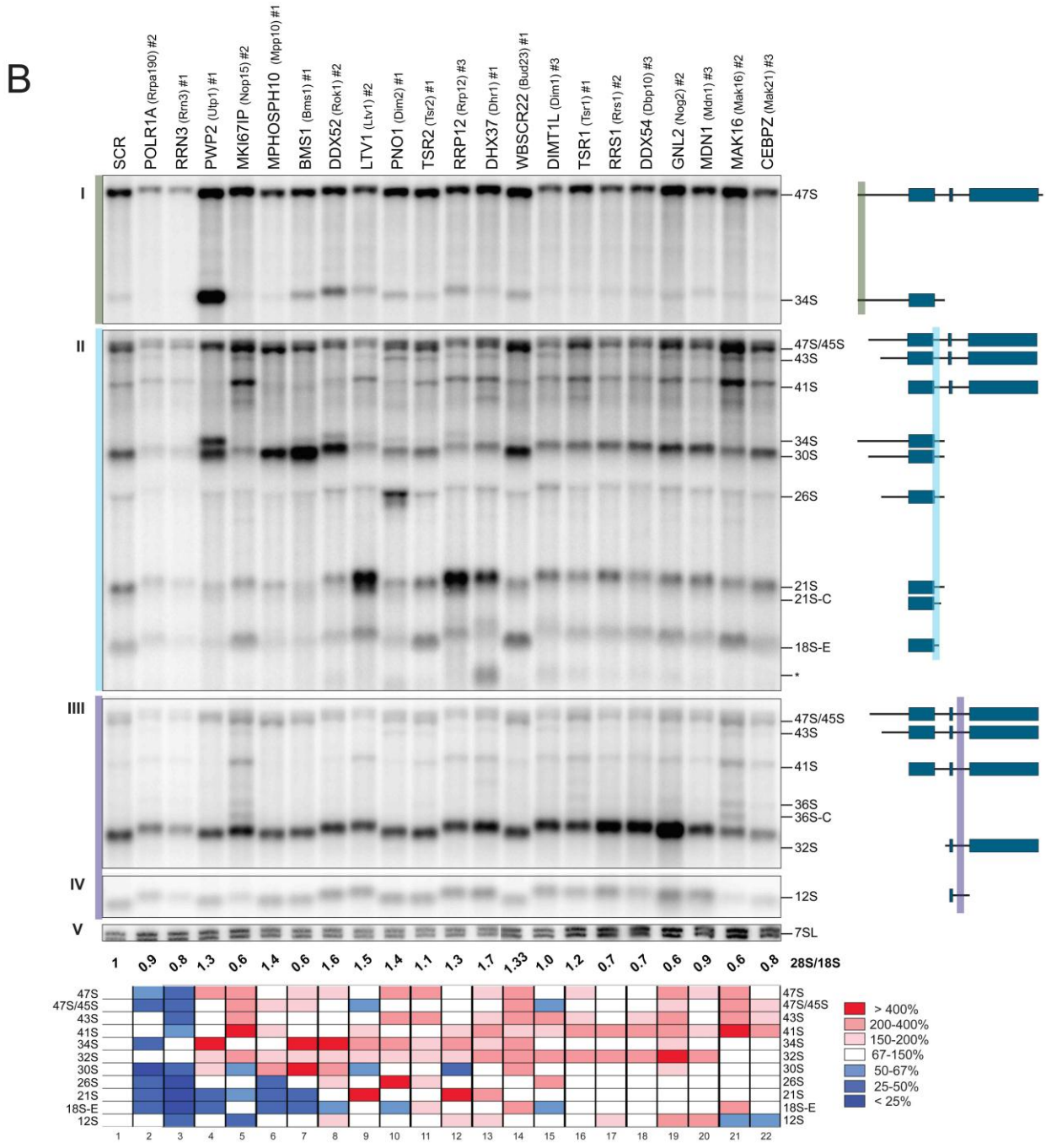
B
SCR
POLR1A (Rrpa190) #2
RRN3 (Rrn3) #1
PWP2 (Utp1) #1
MKI67IP (Nop15) #2
MPHOSPH10 (Mpp10) #1
BMS1 (Bms1) #1
DDX52 (Rok1) #2
LTV1 (Ltv1) #2
PNO1 (Dim2) #1
TSR2 (Tsr2) #1
RRP12 (Rrp12) #3
DHX37 (Dhr1) #1
WBSCR22 (Bud23) #1
DIMT1L (Dim1) #3
TSR1 (Tsr1) #1
RRS1 (Rrs1) #2
DDX54 (Dbp10) #3
GNL2 (Nog2) #2
MDN1 (Mdn1) #3
MAK16 (Mak16) #2
CEBPZ (Mak21) #3
I
II
IIII
IV
V
47S
34S
47S/45S
43S
41S
30S
26S
21S
21S-C
18S-E
*
36S
36S-C
32S
12S
7SL
1 0.9 0.8 1.3 0.6 1.4 0.6 1.6 1.5 1.4 1.1 1.3 1.7 1.33 1.0 1.2 0.7 0.7 0.6 0.9 0.6 0.8
28S/18S
> 400%
200-400%
150-200%
67-150%
50-67%
25-50%
< 25%

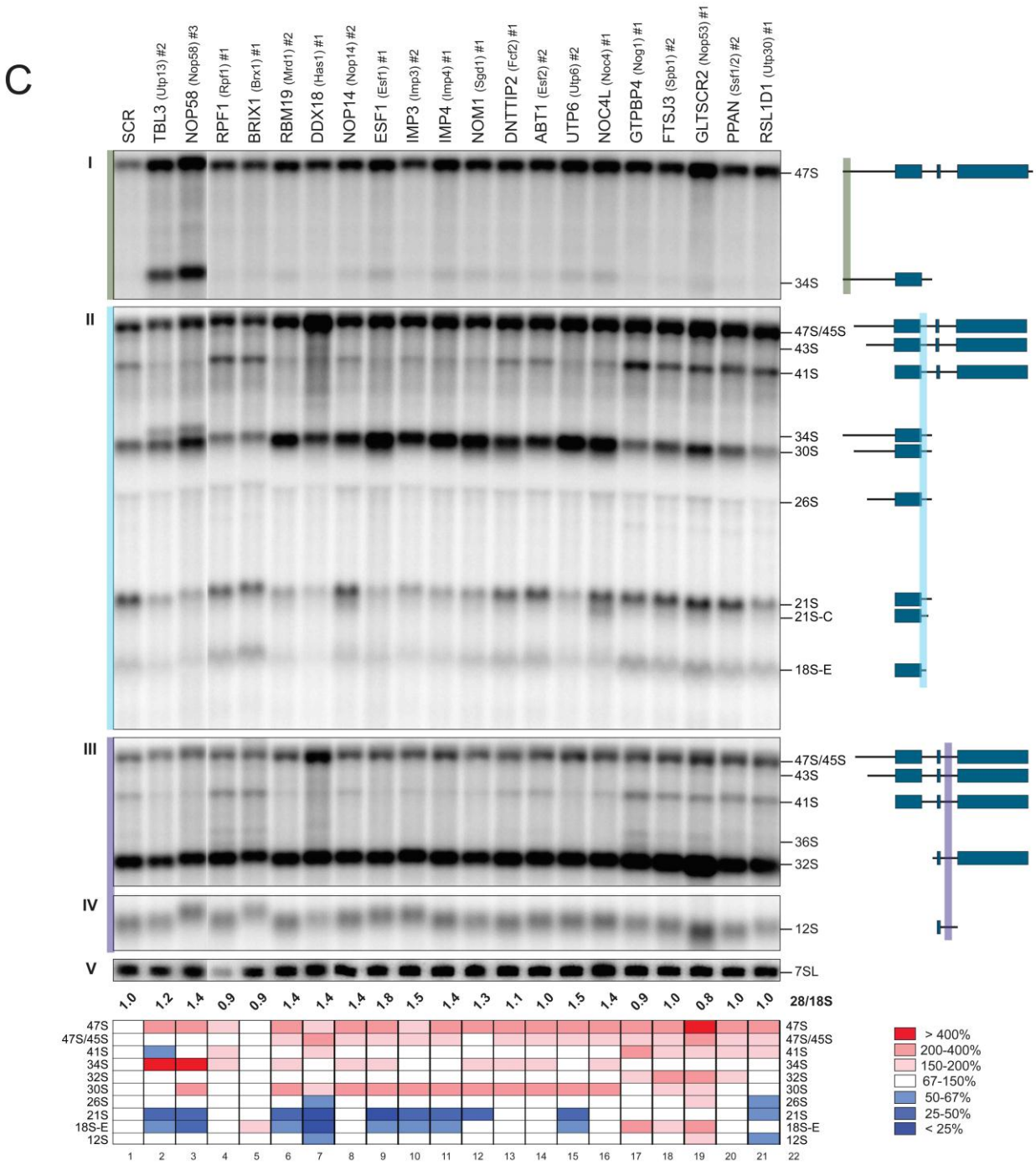

Figure S3. Involvement in Pre-rRNA Processing of 11 Human Genes without a Yeast Homolog and 39 Human Genes with a Yeast Ribosome Assembly Factor Homolog, Related to Figure 3

Analysis of pre-rRNA processing by Northern blotting. Total RNA was extracted from HeLa cells treated for 3 d with a siRNA specific to the target gene, 5 µg was separated by denaturing gel electrophoresis and hybridized with probes (see Fig 1B). As a control, a non-targeting siRNA (SCR) was used. RNAs were resolved on agarose gels with the exception of the 7SL, which was analyzed on acrylamide and provides a loading control. A schematic of the pre-rRNAs detected is provided. siRNA sequences (#1 to #3) are listed in Table S7. The 28S/18S

ratio was calculated from Agilent electropherograms. Bands were quantitated with a Phosphorimager (Fuji FLA-7000) and converted into a heatmap. The signal was standardized to SCR and corrected for loading with the 7SL.

A 11 human genes. RPL26, NCL, UBTF and TEX10 samples were loaded as controls.

Panels I and II, 5' ETS probe; panel III, ITS1 probe; panels IV and V, ITS2 probe; panel VI, probe LD2132; panel VII, probe LD2133. Panels VIII and IX show the large mature rRNAs on an ethidium bromide stained gel.

B 21 human genes with a yeast homolog. The yeast homolog is indicated in brackets. POLR1A and RRN3, both primarily involved in RNA synthesis, were loaded as controls.

Panels I, 5' ETS probe; panel II, ITS1 probe; panels III and IV, ITS2 probe; panel V, probe LD2133.

C 20 human genes with a yeast homolog. Hybridizations as in panel B.

A Human proteins without a yeast homolog

Proteins involved in early processing steps:

Cells depleted for DUSP11 and NOL7 strongly accumulate the 47S primary transcript and 34S RNA, indicating these proteins act at cleavage sites 01, A0 and 1 (panels I and III, lanes 5-6). DUSP11-depleted cells further accumulated a 5'-ETS spacer fragment (+1-01, panel II, lane 5). An increase in 34S was also detected upon the depletion of SF3B14, SRFBP1, NGDN and ZCCHC9 (panel I, lanes 7, 10, 12 and 14). However, in these cases the primary transcript did not accumulate significantly; rather, for SRFBP1 and NGDN, it was the 30S pre-rRNA that became more abundant upon depletion, indicating that cleavages at A0 and 1 are preferentially affected (panel III, lanes 10 and 12). This was also the case for RRP7A (panel III, lane 11). Cells depleted for NOP16 were more abundant in 41S pre-rRNA, indicative of impaired cleavage at site 2 (panel III, lane 9).

Proteins involved in 18S rRNA maturation:

In addition to its effect on 34S accumulation, depletion of ZCCHC9 led to a striking increase in the amount of 21S (panel III, lanes 14), indicating that ZCCHC9 is involved in 18S rRNA maturation. Depletion of SFRS3 and C8orf59 also led to the accumulation of the 21S. For SFRS3, ZCCHC9 and C8orf59, the shorter 21S intermediate (21S-C), typically detected in RPS3-depleted cells (see Fig 1C), was also detected (panel III, lanes 13-15; best seen for ZCCHC9. See RNA exosome role in ITS1 processing. Reduced levels of NOP16 also led to the accumulation of the 18S-E pre-rRNA, a form of 18S rRNA extended by 24 nt at the 3'-end.

Proteins involved in 28S rRNA maturation:

The depletion of THYN1 led to a moderate accumulation of 32S pre-rRNA, similar to what is seen in cells depleted for the ITS2 processing factor TEX10 (panel IV, lanes 8 and 16 and Castle et al., 2012).

B, C Human genes with a yeast homolog

Proteins involved in early processing steps:

Most of the 39 proteins described are involved in early pre-rRNA nucleolar cleavages, as shown by the accumulation of the 47S pre-rRNA. This was particularly evident for GLTSCR2/Nop53 (C, panel I, lane 19). Depletion of PWP2/Utp1, BMS1/Bms1, DDX52/Rok1, TBL3/Utp13 and NOP58/Nop58 and, to a lesser extent, that of four other gene products, led to the accumulation of the aberrant 34S RNA, indicative of cleavage inhibition at 01, A0 and 1 (B, panels I and II, lanes 4, 7-8 and C, same panels, lanes 2-3). MKI67IP/Nop15 and MAK16/Mak16 appeared to be primarily required for cleavage at site 2, as shown by the accumulation of the 41S pre-rRNA (B, lanes 5 and 21). Seven other genes products were also notably involved in processing at site 2: DHX37/Dhr1, TSR1/Tsr1, RRS1/Rrs1, DDX54/Dbp10, GNL2/Nog2, CEBPZ/Mak21 and GTBP4/Nog1. The depletion of BMS1/Bms1 and, to a lesser extent, that of 14 other gene products, led to the accumulation of the 30S (B, panel II, lane 7), indicating a requirement for cleavages at sites A0 and 1. The 26S, resulting from uncoupling at cleavage sites A0 and 1, was particularly abundant in cells deprived of PNO1/Dim2, as well as DIMT1L/Dim1 (B, panel II, lanes 10 and 15).

Proteins involved in 18S rRNA maturation:

Cells lacking LTV1/Ltv1, RRP12/Rrp12 or DHX37/Dhr1 strongly accumulated the 21S (B, panel II, lanes 9, 12 and 13). For LTV1/Ltv1, RRP12/Rrp12, 21S-C was also detected. The 21S-C was also accumulated upon depletion of NOP14/Nop14 and NOC4L/Noc4 (C, panel II, lanes 8 and 16). Depletion of WBSCR22/Bud23, MAK16/Mak16, TSR2/Tsr2, GTPBP4/Nog1 or GLTSCR2/Nop53 led to the accumulation of the late 18S rRNA intermediate, the 18S-E (B, panel II, lanes 11, 14, 21 and C, panel II, lanes 17, 19).

Proteins involved in 28S rRNA maturation:

ITS2 processing was most obviously affected by the depletion of GNL2/Nog1, leading to the accumulation of 32S (B, panel III, lane 19); 10 other gene products were also involved in this processing. The involvement of GNL2/Nog1 in ITS2 processing was also manifested by the accumulation of the 12S, a species that also accumulated upon depletion of MDN1/Mdn1 and GLTSCR2/Nop53 (B, panel IV, lanes 19-20 and C, same panel, lane 19). Finally, several non-canonical species were detected. For example, a truncated 18S rRNA fragment in cells depleted for DHX37 (B, panel II, lane 13, see *) and extended versions of the 32S pre-rRNA (36S and 36S-C) typically detected in RPL26-defective DBA patients for MKI67IP and MAK16 (B, panel III, lanes 5 and 21 and see Figs 3 and 4).

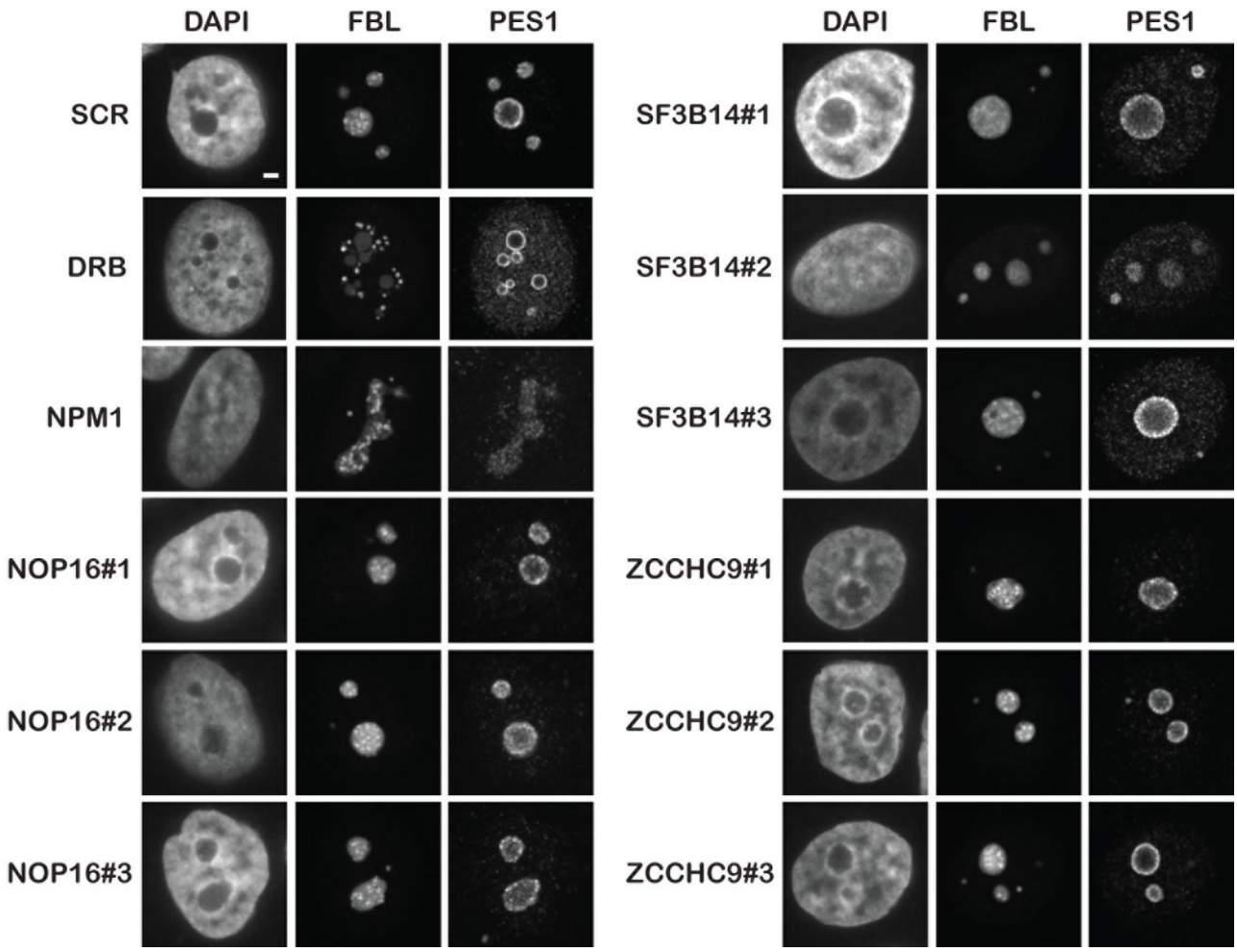

Figure S4. Human Genes without a Yeast Homolog Do Not Grossly Affect Nucleolar Structure, Related to Figure 4

To test for potential effects on nucleolar structure, the 11 proteins were depleted in HeLa cells stably expressing the dense fibrillar component (DFC) marker Fibrillarin (FBL) fused to GFP. Following a 3 d depletion, cells were fixed and immunolabeled with an antibody specific to Pescadillo (PES1), to detect the granular component (GC) of the nucleolus, and imaged by spin disc confocal microscopy. As a control for the disruption of nucleolar structure, the antitumor agent 5,6-Dichlorobenzimidazole 1- β -D-ribofuranoside (DRB) was added to cells. DRB treatment led to the formation of small fibrillarin foci extruding from the main nucleolar volume (counterstained with DAPI), while the GC component PES1 was partially relocated to the nucleoplasm and formed striking perinucleolar rings. Depletion of the control gene nucleophosmin (NPM1) also led to profound nucleolar reorganization with the formation of beaded necklaces. None of the tested proteins showed any gross alteration in nucleolar structure (shown for 3 genes and data not shown). In some instances, PES1 was partially relocated to the nucleoplasm, as seen upon SF3B14 depletion, and to a lesser extent with other genes (data not shown). Scale bar, 2 μm.

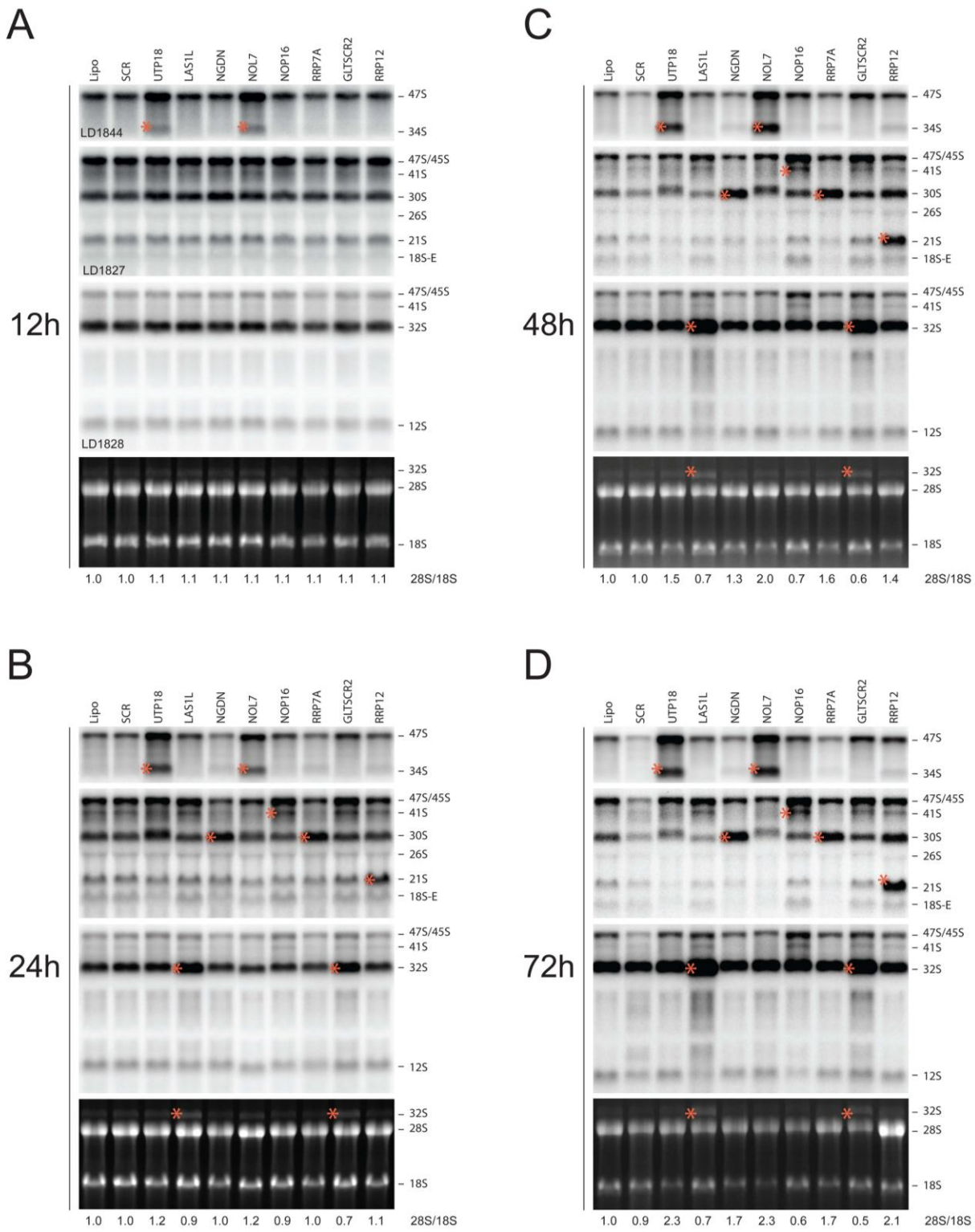

Figure S5. Pre-rRNA Processing Inhibitions Are Early Defects Detected as Soon as 24 hr, or Even 12 hr, after Depletion, Related to Figure 5

HCT116 p53 +/+ cells were depleted for the target genes in a time course analysis. Total RNA was extracted at the indicated time points and analyzed by Northern blotting. The mature rRNAs are shown on an ethidium bromide stained gel. Untreated (Lipo, lipofectamine) cells and cells treated with SCR siRNA were loaded as

controls. On relevant panels, a star highlights the RNA species diagnostic of the defect. 28S/18S ratio determined from Agilent electropherograms. **A** 12 h; **B** 24 h; **C** 48 h; **D** 72 h.

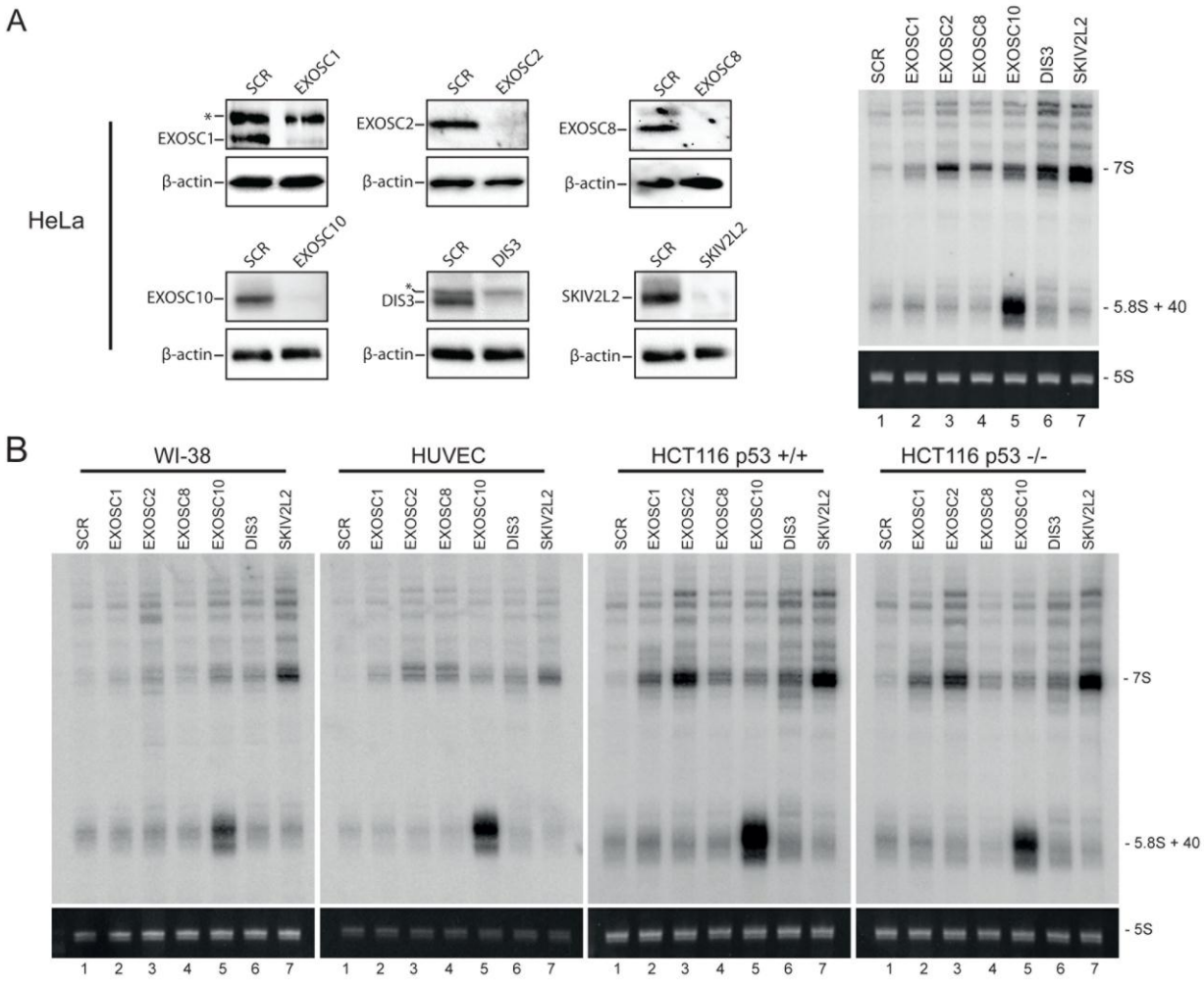

Figure S6. The Requirement for Exosome Subunits and Cofactors in ITS2 Processing Is Conserved in Different Cell Types, Related to Figure 6

A HeLa cells. Select exosome subunits and cofactors were depleted for 3 d in HeLa cells. Total protein was analyzed by Western blotting (left panels) with antibodies specific to the subunits and β-actin as loading control. In the EXOSC1 and DIS3 panels, a star denotes an unspecific cross-reacting band. Total RNA (5 μg) was analyzed by Northern blotting and hybridized with probe LD2079 (right panels). The 5S rRNA detected by ethidium bromide staining provides a loading control.

B WI-38, HUVEC, HCT116 p53 +/+ and HCT116 p53 -/- cells. Indicated cell types were depleted as in panel A. For all cell types, but HUVEC, 3 μg total RNA was loaded; 1 μg was loaded for HUVEC.

SUPPLEMENTAL EXPERIMENTAL PROCEDURES

Phosphorimager Quantification

Northern blots were exposed to Fuji imaging plates (Fujifilm) and signals were acquired with a Phosphorimager (FLA-7000, Fujifilm). A calibration set (Fig 1) was loaded on each gel. The following rRNA fragments were quantified using MultiGauge (v3.1): the 47S pre-rRNA and aberrant 34S (with the 5' ETS probe LD1844); the 47S/45S, 41S, 30S, 26S, 21S and 18-E pre-rRNAs (ITS1 probe LD1827); and the 32S and 12S (ITS2 probe LD1828). Each gel lane and RNA band were identified manually. The background was set automatically using a polygonal lane with settings H ratio= 10 and V ratio= 75 and was then manually curated. The dataset was assembled in Excel and integrated by hierarchical clustering with "R" (http://www.r-project.org/index.html).

Mature rRNA Quantification

The 28S/18S ratio was determined using the Agilent RNA 6000 nano kit (REF 5067-1511) on a BioAnalyzer 2100 (Agilent).

Western Blotting

For immunoblotting, protein lysates corresponding to $6.0x10^4$ cells were prepared as described in Castle et al., 2010. Protein concentration was evaluated with the Bradford assay (Bio-Rad). Total protein was separated by SDS–PAGE (Nu-Page, Invitrogen), transferred to PVDF (GE Healthcare) and analyzed by Western blotting (ECL, ThermoScientific). The following antibodies were used: ExoSC2 (Bethyl Laboratories), ExoSC8 (Abcam), ExoSC10 (Sigma-Aldrich), DIS3 (Bethyl Laboratories), β-ACTIN and p53 (Santa Cruz biotechnology). The ExoSC1 and SKIV2L2 antibodies were kindly provided by Dr Nicholas J. Watkins (Sloan et al., 2013). Images were acquired and processed with a ChemiDoc MP (Bio-Rad).

Shotgun qPCR

The efficiency of siRNA-mediated knockdown was determined by qPCR using a shotgun approach (8.2% of siRNA depletions tested altogether, see Fig S2), using GAPDH as an endogeneous control. Reactions were performed as previously described (Schillewaert et al., 2012). Primer sequences are listed in Table S9. Triplicate reactions were performed for each sample. Data were analyzed with the software StepOne (version 2.1) from Applied Biosystems (Life Technologies). The comparative threshold cycle method ($\Delta\Delta CT = \Delta C_T target - \Delta C_T scrambled$) was used to determine the relative abundance of mRNA transcripts.

Selection of 625 Targets

The list of candidate proteins was generated from the human nucleolar databases (Andersen et al., 2002; Scherl et al., 2002) and expanded using the bovine and plant *Arabidospis thaliana* nucleolar proteomes (Patel et al., 2010; Pendle et al., 2005), with selected entries from the Gene Ontology database (GO0042254 and GO0006364). A compilation of the yeast ribosome processing factors was generated mainly from Fromont-Racine et al., 2003; Kressler et al., 1999; Strunk and Karbstein, 2009. Human homologs were retrieved using a blastp search (expected p value < 10^{-15}). Note that a few yeast proteins have multiple human counterparts (especially helicases) and that several (30 proteins) do not have human homologs. From this assembled list of ~800 human proteins with putative functions in pre-rRNA processing we excluded all ribosomal proteins, as they were already described (O'Donohue et al., 2010), or are currently studied elsewhere, several histones and other proteins with conflicting subcellular localization. The final list comprised 625 candidates.

Generation of Heatmaps and Functional Cluster

The dataset was normalized as follows: each rRNA species was normalized to its corresponding fragment in the SCR sample loaded on the same gel. In the functional clustering analysis, all the calibration sets clustered consistently, providing validation of the grouping approach. The dataset was assembled into a matrix in Excel (see www.ribogenesis.com) and hierarchical clustering was done with the R freeware using the Gplots and plotrix packages (www.r-project.org/). The pre-RNA profiles obtained for each gene with all three independent siRNAs were systematically inspected in the functional cluster (see www.ribogenesis.com). Pre-rRNA processing profiles were considered similar when they were within a functional neighborhood of 10 genes.

Microscopy

A stable HeLa cell line, expressing a GFP-FBL fusion was used (a kind gift from Prof. D Hernandez-Verdun, Institut Jacques Monod, Paris). siRNA-mediated depletion was done as described above. As control, cells were treated with DRB (0.1 mM, 2 h). After 72h of depletion, cells were fixed with 2% formaldehyde for 15 min, and permeabilized with 2% BSA/0.2% Triton X-100 for 10 min. Unspecific binding was blocked with PBS/2% BSA for 30 min. PES1 was detected with a 1:1000 dilution of anti-Pes1 antibody (Ascenion), incubated for 2h at RT in a humidified chamber. After washing with PBS/2% BSA, the Alexa fluor 568 anti-rat (Invitrogen, A11077) secondary antibody was incubated in a dilution of 1:1000 for 2h at RT in a humidified chamber. Cells were washed with PBS and DNA was stained with 100 ng/mL DAPI (Sigma) for 10 min. Images were acquired using MetaMorph and a spin disc microscope (Yokogawa CSU-X1) with a HQ^2 Coolsnap Roper camera and a Plan-

Apochromat 100x, 1.46 numerical aperture objective lens. Exposure for DAPI, GFP and TxRed was 60 ms, 30 ms and 2 s, respectively.

Time Course Analysis

siRNA transfection: HCT116 cells were reverse-transfected as described for HeLa in 6-well plate but the number of cells seeded per well were modified according to the depletion time ($5x10^5$ cells for 12h depletion, $4x10^5$ cells for 24h, $3x10^5$ cells for 48h and $1.5x10^5$ cells for 72h). RNA were extracted using TRI reagent (Life Technologies). For Annexin V and caspase 3/7 assays (apoptosis assays), cells were transfected as above but in a 96-well format ($30x10^3$ cells for 12-h depletion, $20x10^3$ cells for 24-h, $10\ x10^3$ cells for 48-h and $5\ x10^3$ cells for 72-h). As a control, cells were treated with 1 µM camptothecin (Sigma). Immunodetection: for protein extraction, cells were washed in PBS 1x and lysed in 300 µl RIPA buffer (25 mM Tris-HCl, pH 7.6, 150 mM NaCl, 1% NP-40, 1% Triton X-100, 1% sodium deoxycholate, 0.1% SDS, supplemented by a protease inhibitor cocktail (Complete, Roche)) for 15 minutes on ice. Lysates were cleared by centrifugation. Proteins were separated by SDS-PAGE on precast gels (criterion TGX 4-20%, Bio-Rad) and transferred to a PVDF membrane (GE healthcare). β-actin and p53 (Santa Cruz biotechnology) antibodies were used to detect both proteins. Signals generated by chemiluminescence (Thermo Scientific) were detected using a ChemiDoc MP system (Bio-Rad) and quantified using ImageLab (Bio-Rad). Apoptosis: three assays were used to estimate the level of apoptosis. In the TUNEL assay, cells were treated according to the manufacturer's instructions (Apo-BrdU TUNEL assay, Life Technologies), stained by propidium iodide to follow the DNA and analyzed by flow cytometry (FACScantoII, BD). Cell-cycle was analyzed using FlowJo (TreeStar). For the Annexin V assay, we used Annexin-V-FLUOS (Roche) and analyzed differentially stained cells by microscopy and manual counting. Images were captured with a wide field fluorescent microscope (Observer.Z1, CoolLED excitation system) and an EC Plan-Neofluar 20x, 0.5 numerical aperture objective lens. For the caspase 3/7 assay, we used the ApoTox-Glo kit (Promega) and a Tecan luminometer plate reader.

SUPPLEMENTAL REFERENCES

Andersen, J.S., Lyon, C.E., Fox, A.H., Leung, A.K., Lam, Y.W., Steen, H., Mann, M., and Lamond, A.I. (2002). Directed proteomic analysis of the human nucleolus. Curr Biol *12*, 1-11.

Castle, C.D., Cassimere, E.K., and Denicourt, C. (2012). LAS1L interacts with the mammalian Rix1 complex to regulate ribosome biogenesis. Mol Biol Cell *23*, 716-728.

Castle, C.D., Cassimere, E.K., Lee, J., and Denicourt, C. (2010). Las1L is a nucleolar protein required for cell proliferation and ribosome biogenesis. Mol Cell Biol *30*, 4404-4414.

Fromont-Racine, M., Senger, B., Saveanu, C., and Fasiolo, F. (2003). Ribosome assembly in eukaryotes. Gene *313*, 17-42.

Kressler, D., Linder, P., and de La Cruz, J. (1999). Protein trans-acting factors involved in ribosome biogenesis in Saccharomyces cerevisiae. Mol Cell Biol *19*, 7897-7912.

O'Donohue, M.F., Choesmel, V., Faubladier, M., Fichant, G., and Gleizes, P.E. (2010). Functional dichotomy of ribosomal proteins during the synthesis of mammalian 40S ribosomal subunits. J Cell Biol *190*, 853-866.

Patel, A.K., Olson, D., and Tikoo, S.K. (2010). Proteomic analysis of bovine nucleolus. Genomics Proteomics Bioinformatics *8*, 145-158.

Pendle, A.F., Clark, G.P., Boon, R., Lewandowska, D., Lam, Y.W., Andersen, J., Mann, M., Lamond, A.I., Brown, J.W., and Shaw, P.J. (2005). Proteomic analysis of the Arabidopsis nucleolus suggests novel nucleolar functions. Mol Biol Cell *16*, 260-269.

Scherl, A., Coute, Y., Deon, C., Calle, A., Kindbeiter, K., Sanchez, J.C., Greco, A., Hochstrasser, D., and Diaz, J.J. (2002). Functional proteomic analysis of human nucleolus. Mol Biol Cell *13*, 4100-4109.

Schillewaert, S., Wacheul, L., Lhomme, F., and Lafontaine, D.L.J. (2012). The Evolutionarily Conserved Protein LAS1 Is Required for Pre-rRNA Processing at Both Ends of ITS2. Mol Cell Biol *32*, 430-444.

Sloan, K.E., Mattijssen, S., Lebaron, S., Tollervey, D., Pruijn, G.J., and Watkins, N.J. (2013). Both endonucleolytic and exonucleolytic cleavage mediate ITS1 removal during human ribosomal RNA processing. J Cell Biol *200*, 577-588.

Strunk, B.S., and Karbstein, K. (2009). Powering through ribosome assembly. RNA *15*, 2083-2104.